AD-755 260

ELECTRONIC STATES IN DISORDERED MATERIALS

M. Silver, et al

North Carolina University

Prepared for:

Army Research Office-Durham
Advanced Research Projects Agency

31 July 1972

DISTRIBUTED BY:

NTIS
National Technical Information Service
U. S. DEPARTMENT OF COMMERCE
5285 Port Royal Road, Springfield Va. 22151

BEST
AVAILABLE COPY

aQ00-9537.4-P

Form Approved
Budget Bureau N. 22-R0293

AD755260

Semi-Annual Technical Report

February 1, 1972 to July 31, 1972

ARPA Order No. 1562

Profram Code No. OD10

Name of Grantee
University of North Carolina at
Chapel Hill

Effective date of Grant
April 1, 1972

Expiration Date
March 31, 1973

Amount of Grant
$32,892

Grant No.
DA-AROD-31-124-71-G52

Principal Investigators
M. Silver and K. S. Dy
Phone No. 919-933-3015

Project Scientist
C. Boghosian
Phone No. 919-286-2285

Short Title: Electronic States in Disordered Materials

Sponsored by

Advanced Research Projects Agency

ARPA Order No. 1562

Approved for public release; distribution unlimited.

Reproduced by
NATIONAL TECHNICAL INFORMATION SERVICE
U S Department of Commerce
Springfield VA 22151

D D C
RECEIVED
FEB 12 1973
B

Theory

(1) Electronic Structure of Disordered Systems.

The study of the electronic structures of one-dimensional disordered arrays of delta-function potentials has provided us with considerable insights into the applicability of the Wu-Dy method[1] to three-dimensional systems. The preprint of a paper containing the results is attached. Extension to three dimensions are now under way. The models considered are those of Henderson[2] and Polk[3]. The function $R_{kk'}$ required in the Wu-Dy method has recently been computed by Chaudhari, Graczyk, and Charbnau[4] for the Henderson model. Their results confirms our original conjecture that considerable fine structures in this function will remain when the lattice becomes amorphous. These fine structures are due to coherent scattering of clusters of atoms with short range order. In order to complete our calculation of the density of states, we need in addition the function $\tilde{W}_{kk'}$, which is the fluctuation in the energy band due to disorder. Since computer effort in this direction is anticipated to be enormous, we are now trying to see if a reasonable analytic approximation is possible.

In our attempt to understand the electronic structure, we have also investigated the tight - binding approach to the problem. We have calculated the density of states of the Henderson model and the Polk model based on the one band hamiltonian $H = \sum V|i\rangle\langle i'|$, where the sum is over all nearest neighbor pairs i and i'. In order to calculate the density of states, we computed the first ten moments of the density of states using the close-walk counting technique. We then derive the density of states by fitting the moments with an expansion in Legendre polynomials. Since the Henderson and Polk models are small enough for the hamiltonian to be diagonalized numerically, we also calculated the exact eigen-values and eigen-states. The density of states derived in this way agree very well with those derived from the moment method. The eigen-states so derived exhibit no localization. In order to produce localization, we made a numerical study of the Anderson model hamiltonian

$$H = \sum_i E|i\rangle\langle i| + \sum_{ii'} V|i\rangle\langle i'|$$

where E fluctuates within the bounds ± W/2. We calculated the localization parameter

$$\alpha = \sum_{i=1}^{N} |a_i|^4 / (\sum_{i=1}^{N} |a_i|^2)^2$$

where the a_i are amplitudes for some particular eigen-states. In a similar study, Edwards and Thouless[5] show that for perfect diamond lattice, the onset of localization is less sharply defined and occurs more easily than in the Anderson theory. For the disordered Henderson model we find that the onset of localization is also not sharply defined and that localization is the same on the average to that in the perfect diamond structure. The extension to more realistic models are now being considered.

(2) Models of Steady State Electron Injection Current into Dense Media.

We have completed our calculations of the field and density dependence of the steady state electron current injected into dense argon, hydrogen, and nitrogen gases. The results are included in a preprint attached.

Experiment

Experimentally, we have concentrated on continuing our experiments on the drift of electrons in dense helium gas. Our results are now in accord with previous experiments, the precipitous drop we reported in our last report is in fact double branching, i.e. a high mobility branch coexisting with a low mobility branch. This was observed before in hydrogen but never in helium and suggest a very long life time for bubble formation at these high densities. A preprint covering these result is attached.

References

(1) K. S. Dy and Shi-Yu Wu, Phys. Rev. B3, 1173 (1971).

(2) D. Henderson, private communication. (see also Bull. Am Phys. Soc. 16, 347 (1971).

(3) D. E. Polk, J. Non-Cryst. Solids 5, 365 (1971).

(4) P. Chaudhari, J. F. Graczyk, and H. P. Charbnau, Phys. Rev. Letters 29, 425 (1972).

(5) J. T. Edwards and D. J. Thouless, private communication.

Electronic Structure of Disordered Systems —
II. One-Dimensional Arrays, Bound Bands*

J. C. Wang and K. S. Dy
Department of Physics, University of North Carolina
Chapel Hill, North Carolina 27514

and

Shi-Yu Wu
Department of Physics, University of Louisville
Louisville, Kentucky 40208

Abstract

The structure of the bound band of a one-dimensional disordered array of attractive δ-function potentials was calculated using the method of Wu and Dy.[1]

I. Introduction

In a previous paper[1] (referred to as I), we presented a method for calculating the electronic density of states in disordered systems. We showed that the method can be easily generalized to systems with structural disorder. Here we applied the method to calculate the density of bound states for an electron in a one-dimensional disordered array of attractive δ-function potentials of a given strength. Other methods of solving this particular problem exist.[2-6] Our purpose here is to illustrate how the method presented in I works and to provide insight for the application of the method to three-dimensional problems.

Although the one-dimensional disordered array is not a topological disordered system, we have not taken the advantage of the sequential numbering of the atomic sites to reduce the problem into an ordered one. We also do not use the closely connected method of relating the energy eigenvalue to the number of nodes in the wavefunction. Thus our method of calculation can be readily extended to two and three dimensions. However, as a basis for comparison, we also calculated the exact density of states by the node counting method of Lax and Phillips.[2]

We shall consider only arrays having short range order as defined by Gubanov[7] in the following way. The distance between each pair of neighboring atoms is taken to be $a(1 + \varepsilon\gamma)$ where a is the average interatomic spacing L/N, L being the length of the chain and N the number of atoms in the chain. The factor ε is a positive number less than one (called the short range order parameter) and γ is a random number having a Gaussian distribution with $\langle\gamma\rangle = 0$, $\langle\gamma^2\rangle = 1$. Makinson and Roberts[3] have computed the density of states of one-dimensional arrays of δ-function potentials with ε ranging from 0 to 0.1. The results presented, however, are for the positive energy region only. In this work we have calculated the energy level distribution in the negative energy region for the same range of ε.

II. Method of Calculation

We use the Green's function formulation presented in I to calculate the density of states. The Hamiltonian we consider is given by

$$H = \frac{p^2}{2m} - \sum_{\ell} V_0 \delta(x - \ell), \tag{2.1}$$

where V_0 is a positive number which defines the strength of the potential and ℓ denotes the atomic sites. The tight-binding wavefunction is taken to be the eigenstate

$$\phi(x - \ell) = \left(\frac{mV_0}{\hbar^2}\right)^{\frac{1}{2}} \exp\left[-\frac{mV_0}{\hbar^2}|x - \ell|\right] \tag{2.2}$$

of

$$h = \frac{p^2}{2m} - V_0\delta(x - \ell) \tag{2.3}$$

with eigenvalue

$$w = -\frac{mV_0^2}{2\hbar^2}. \tag{2.4}$$

For simplicity we set w equal to -1. Using (2.2) one can easily compute the matrix elements of the total Hamiltonian:

$$H_{\ell\ell'} = w\delta_{\ell\ell'} + 2w \sum_{\ell''\neq\ell'} \exp\{-\frac{mV_0}{\hbar^2}(|\ell'' - \ell| + |\ell'' - \ell'|)\}. \tag{2.5}$$

Defining the position ℓ by a dimensionless parameter $\tilde{\ell} \equiv \ell/a$, we get

$$H_{\tilde{\ell}\tilde{\ell}'} = w\delta_{\tilde{\ell}\tilde{\ell}'} + 2w \sum_{\tilde{\ell}''\neq\tilde{\ell}} \exp\{-A(|\tilde{\ell}' - \tilde{\ell}| + |\tilde{\ell}'' - \tilde{\ell}'|)\}, \tag{2.6}$$

where $A \equiv \frac{mV_0}{\hbar^2}a$. Henceforth we shall omit the ˜ sign over the ℓ's. The parameter A is equivalent to ε^{-1} in Lax and Phillips' notation.

In the formulation of I we need the following quantities:

$$R_{kk'} \equiv N^{-1} \sum_{\ell} e^{i(k-k')\ell} - \delta_{kk'}, \tag{2.7}$$

$$\tilde{V}(k) \equiv N^{-1} \sum_{\ell L} H_{\ell,\ell-L}\, e^{ikL}, \tag{2.8}$$

$$U(\ell,k) \equiv \sum_{L} H_{\ell,\ell-L}\, e^{ikL} - \tilde{V}(k), \tag{2.9}$$

$$\tilde{W}_{kk'} \equiv N^{-1}\sum_{k''} (I + R)^{-1}_{kk''} \, e^{i(k''-k')\ell} \, U(\ell,k'). \quad (2.10)$$

Typical curves of R, $\tilde{V}$, U and $\tilde{W}$ are shown in Figs. 1-3. The matrix $(I + R)^{-1}$ needed to calculate $\tilde{W}_{kk'}$ is inverted from I + R using a computer.

Using the computed values of $\tilde{V}(k)$ and $\tilde{W}_{kk'}$, we calculated the Green's function by the direct summation of the band propagator expansion:

$$\tilde{G}(k,z) = 1/(z - \tilde{V}(k) - \Sigma(k,z)). \quad (2.11)$$

where

$$\Sigma(k,z) = \tilde{W}_{kk} + \sum_{k'\neq k} \tilde{W}_{kk'}\tilde{G}(k',z)\tilde{W}_{k'k} + \ldots.. \quad (2.12)$$

We truncated the series for the proper self-energy Σ at the second term as shown in (2.12) and solved for $\tilde{G}$ self-consistently using a computer. The density of states was calculated from $\tilde{G}$ by

$$dN(E)/dE \equiv n(E) = -\frac{1}{\pi}\sum_{k} \text{Im}\, \tilde{G}(k,z \to E + i0^{+}). \quad (2.13)$$

III. Results and Discussion

In Fig. 1, the curve for $|R_{kk'}|^2$ shows considerable structures. These structures are closely related to coherent scattering from clusters of atoms in the array. P. Chaudhari, J. F. Graczyk and H. P. Charbau[8] recently calculated the quantity $|R_{kk'}|^2$ (FF^* in their notation) for a three-dimensional random network model of a tetrahedrally coordinated amorphous solid. Their result shows similar structures in the $|R_{kk'}|^2$ curve but with less intensity in the local maxima compared with our one-dimensional random array.

In Fig. 2, the $\tilde{V}(k)$ curve (solid line) is the average of $\sum_L H_{\ell,\ell-L}\, e^{ikL}$ over all sites ℓ, i.e., it is the energy dispersion of the electron in an 'average crystal'. The approximation $\tilde{G}(k,z) \approx 1/(z-\tilde{V}(k))$ gives essentially the energy band of the perfectly ordered array and, therefore, is a poor approximation for the tail states. The structures in the $U(\ell,k)$ curve, for a given k value, presented in Fig. 3

represent the deviation of $\sum_L H_{\ell,\ell-L}\, e^{ikL}$ from $\tilde{V}(k)$ from site to site and arise because of the disorder. Note that the fluctuations are of the same order of magnitude as the band-width given by $\tilde{V}(k)$ alone. In Fig. 2 we see that the transformation of $U(\ell,k)$ to $\tilde{W}_{kk'}$ (dashed line) reduces the fluctuations to values much smaller than the band width of $\tilde{V}(k)$. This reduction is due to the short-range order in the array considered.

In Fig. 4(a) and (b) we show (solid lines) the calculated density of states, $dN(E)/dE$, for a chain of 50 particles with short-range order parameter ε equal to 0.05 and 0.1. In Fig. 5(a) and (b) we show (solid lines) the corresponding integrated density of states, $N(E)$. In all these cases, the quantity A which determines the degree of overlap of the neighboring wavefunctions is taken to be 10. As a comparison, we plotted in the same figures the exact results obtained by the node counting method of Lax and Phillips (histograms in Fig. 4 and dots in Fig. 5). The positions of the band edges for the perfectly ordered system are indicated by arrows in the figures. From Figs. 4 and 5 one can see the gradual spreading of the allowed band as the disorder increases. Because of the small size of the arrays considered, the exact density of states shows considerable fine structures. In Fig. 6 we show the exact density of states for a bigger sample consisting of 2000 particles. It is evident that the fine structures diminish as the sample size becomes larger. The density of states calculated by our method using the 50-particle sample is smoothed out because of the approximation used in summing the proper self-energy series. The finite imaginary part of the proper self-energy gives rise to a broad Lorentzian rather than a delta function at each eigenvalue in the density of states.

Ideally, the comparison of results should be made for a very large sample. Because the computer time[9] for the present method increases with sample size N roughtly as N^3, no sample larger than 50 particles were attempted. Nevertheless, Figs 4 and 5 show that on the average the band tails are quite well reproduced by our present calculations. The larger discrepancies actually occur at the center of the band. The reason is that states at the center of the band are quite extended (see Fig. 7b), and as the disorder increases, the overlap of the wavefunctions can become quite large, thus introducing larger errors in the tight-binding approximation.

We conclude that using the present method, the band tails of disordered systems with short range order can be calculated quite accurately. However, because of the large computer time involved the application to three dimensional systems could best be done by introducing analytic approximations to the functionals $R_{kk'}$ and $\tilde{W}_{kk'}$ for an infinite system.

*Work supported by the Materials Research Center, UNC, under Contract number DAHC-15-67-C-0223 from the Advanced Research Projects Agency and a grant monitored by the U. S. Army Research Office - Durham under Grant number DA-AROD-31-71-G52.

References

1. K. S. Dy and S. Y. Wu, Phys. Rev. B3, 1173 (1971).
2. M. Lax and J. C. Phillips, Phys. Rev. 110, 41 (1958).
3. R. E. B. Makinson and A. P. Roberts, Australian J. Phys. 13, 437 (1960).
4. A. P. Roberts and R. E. B. Makinson, Proc. Phys Soc. 79, 630 (1962).
5. J. F. Reading and J. L. Siegel, Phys. Rev. B5, 556 (1972).
6. T. P. Eggarter, Phys. Rev. B5, 3863 (1972).
7. A. I. Gubanov, Ah. Eksp. Teor. Fiz. 26, 139 (1954).
8. P. Chaudhari, J. F. Graczyk and H. P. Charbnau, Phys. Rev. Letters 29, 425 (1972).
9. With IBM 360/175, the actual calculation time is about one minute for a 50-particle system.

Figure Captions

Figure 1 $|R_{kk'}|^2$ as a function of $|k-k'|$ for 50 δ-function potentials with short range order parameter $\varepsilon = 0.05$.

Figure 2 Typical $\tilde{V}(k)$ curve (solid line) and the real part of $\tilde{W}(k',k)$ curve (dash line) with $k' = -4\pi/5$ for a linear chain of 50 δ-function potentials with $\varepsilon = 0.05$ and overlap parameter $A = 10$. The imaginary part of $\tilde{W}(k',k)$, which is not shown here, has the same order of magnitude as Re $\tilde{W}(k',k)$.

Figure 3 Real (solid line) and imaginary (dash line) parts of typical $U(\ell,k)$ curve with $k = -2\pi/5$ for 50 δ-function potentials with $\varepsilon = 0.05$ and $A = 10$. w is the eigen-energy of the bound state of a single δ-function potential.

Figure 4 Density of states calculated with the Dy-Wu method (solid lines) and the node-counting method (histograms) for 50 δ-function potentials with $A = 10$ and (a) $\varepsilon = 0.05$ and (b) $\varepsilon = 0.1$. Arrows indicate the band edges for the perfectly ordered system. The bound-state energy of a single δ-function potential is chosen to be zero.

Figure 5 Integrated density of states calculated with the Dy-Wu method (solid line) and the node-counting method (dots) for 50 δ-function potentials with $A = 10$ and (a) $\varepsilon = 0.05$ and (b) $\varepsilon = 0.1$. Arrows indicate the band edges for the perfectly ordered system.

Figure 6 Density of states calculated with the node-counting method for 2000 δ-function potentials with (a) $\varepsilon = 0.05$ and (b) $\varepsilon = 0.1$.

Figure 7 Eigenstates for (a) $E = 4.66 \times 10^{-4}|w|$, (b) $E = -0.1 \times 10^{-4}|w|$, and (c) $E = -7.35 \times 10^{-4}|w|$ for a 50-particle system with $\varepsilon = 0.1$. The eigenstates $\psi_E(x) = \sum_\ell a_\ell(E)\phi(x - \ell)$ are obtained by finding the eigenvectors of the Hamiltonian matrix. Only the amplitudes, a_ℓ, are plotted in the figure.

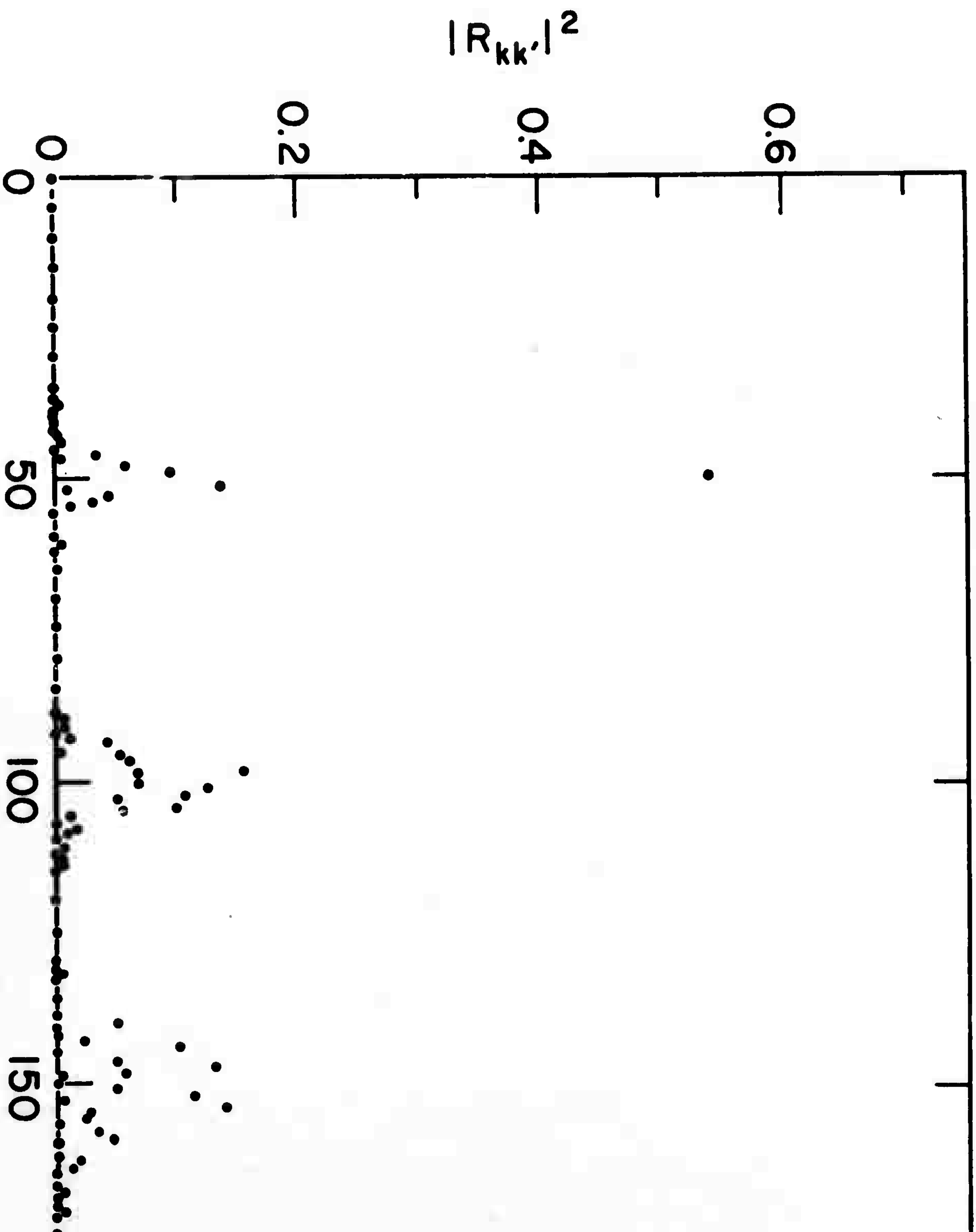

$|R_{kk'}|^2$
0
0.2
0.4
0.6
$|k-k'|(2\pi/50a^{-1})$
0
50
100
150
200

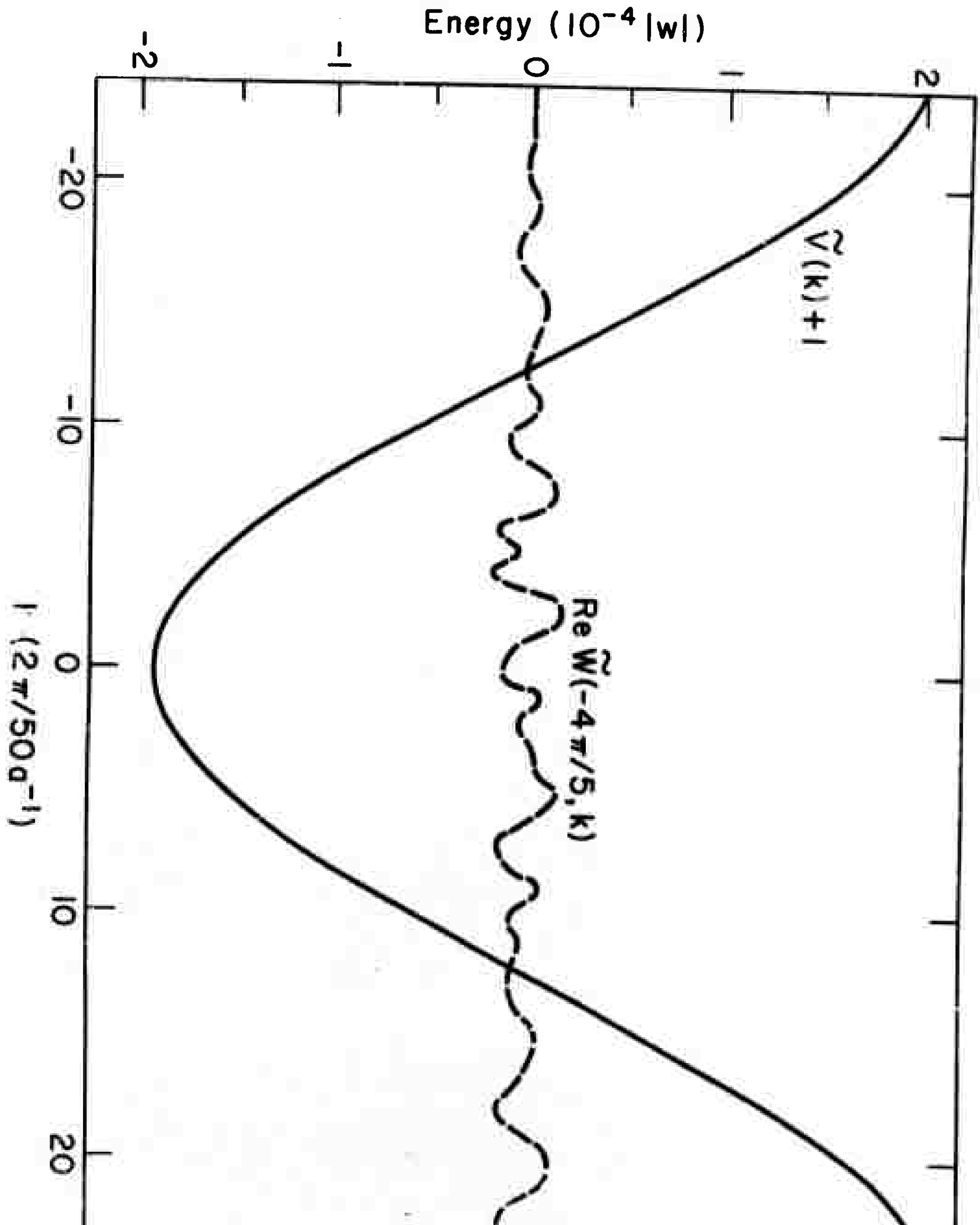
Energy ($10^{-4}|w|$)
-2
-1
0
1
2
-20
-10
0
10
20
$\tilde{V}(k)+1$
Re $\tilde{W}(-4\pi/5,k)$
l ($2\pi/50a^{-1}$)

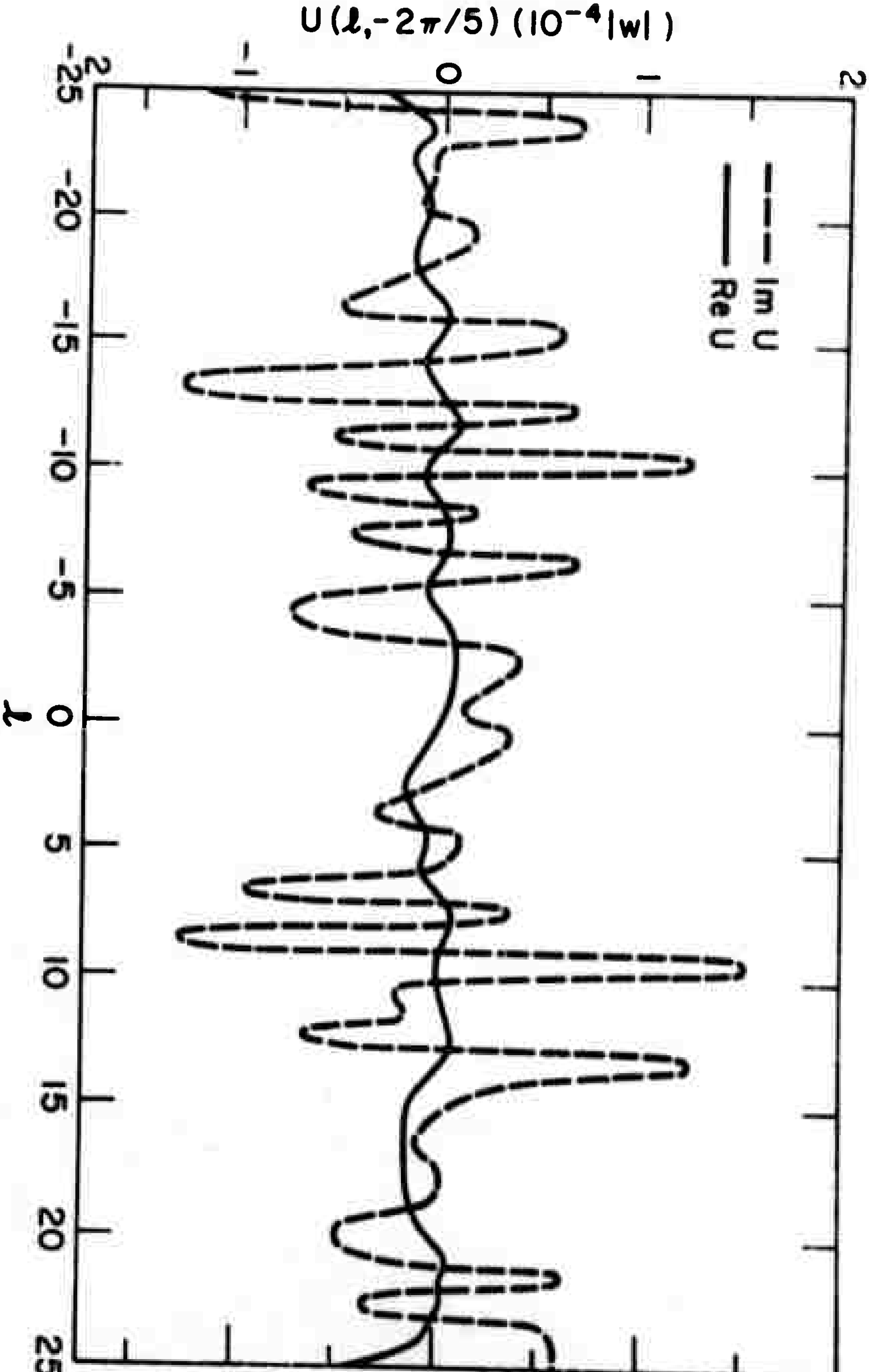

U(ℓ,-2π/5) (10⁻⁴|w|)
Im U
Re U
ℓ
-25
-20
-15
-10
-5
0
5
10
15
20
25
-2
-1
0
1
2

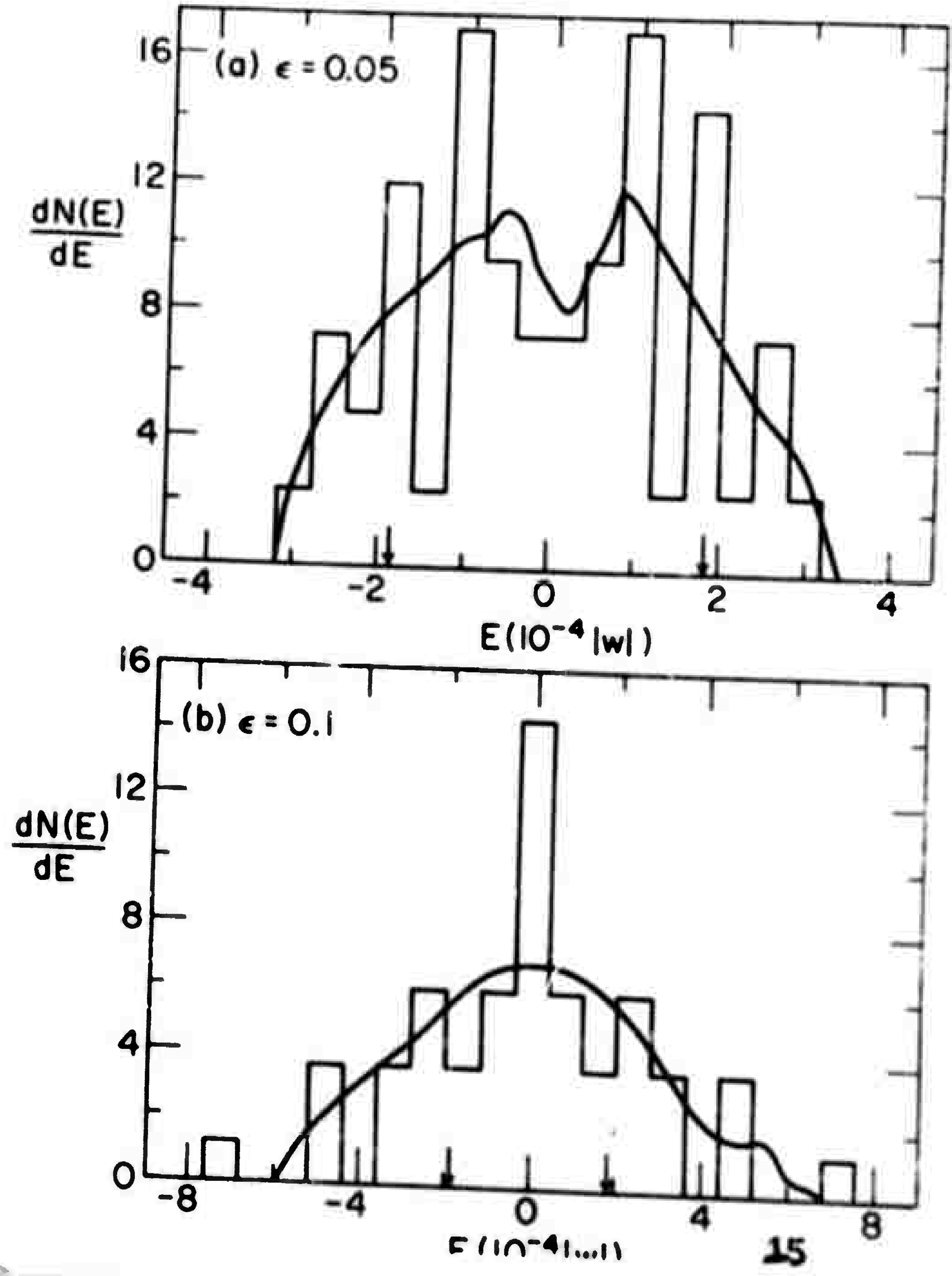

(a) ϵ = 0.05
dN(E)/dE
16
12
8
4
0
-4
-2
0
2
4
E(10⁻⁴ |W|)
(b) ϵ = 0.1
dN(E)/dE
16
12
8
4
0
-8
-4
0
4
8

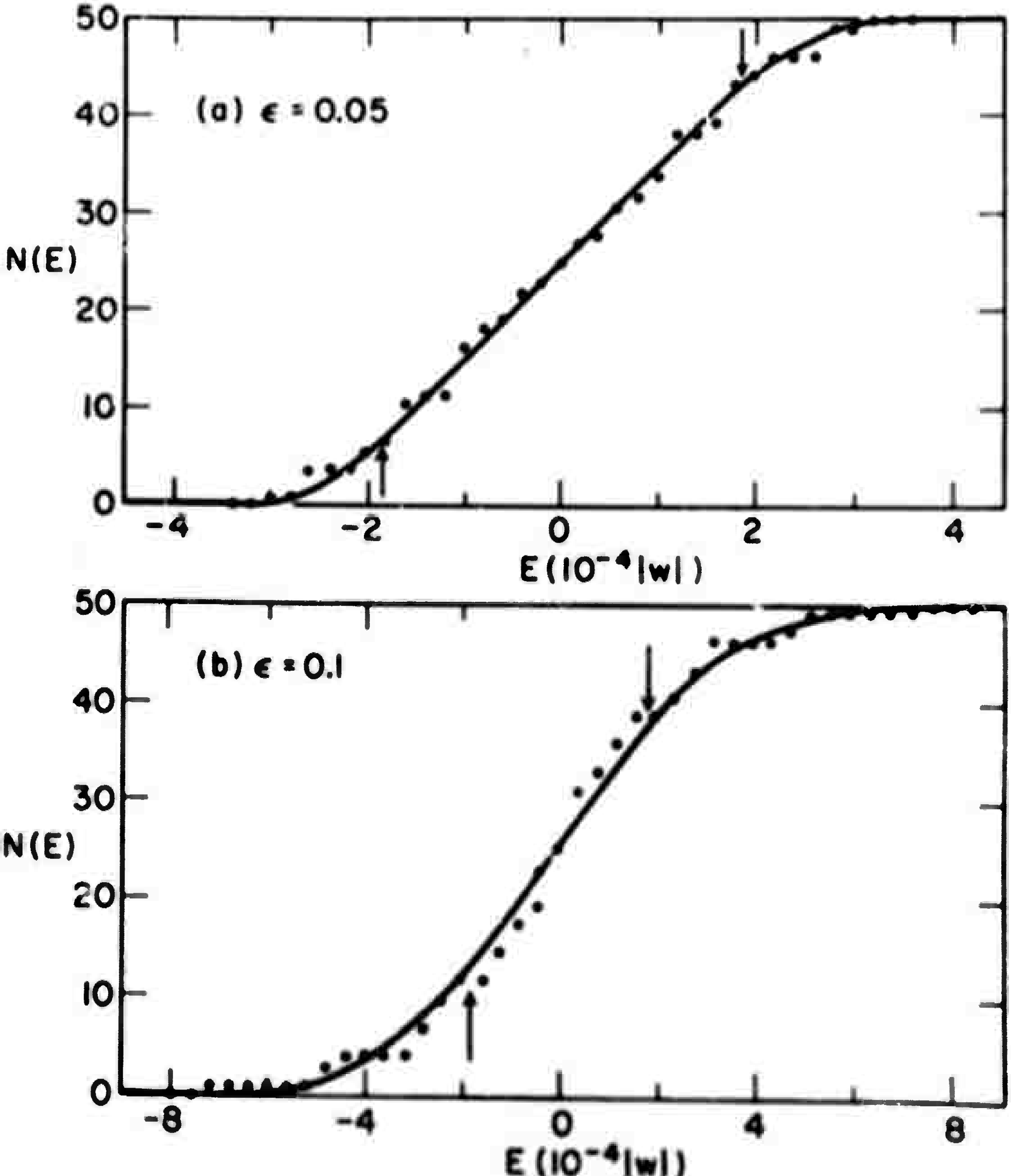

(a) ϵ = 0.05
N(E)
E(10^{-4}|w|)
(b) ϵ = 0.1
N(E)
E(10^{-4}|w|)

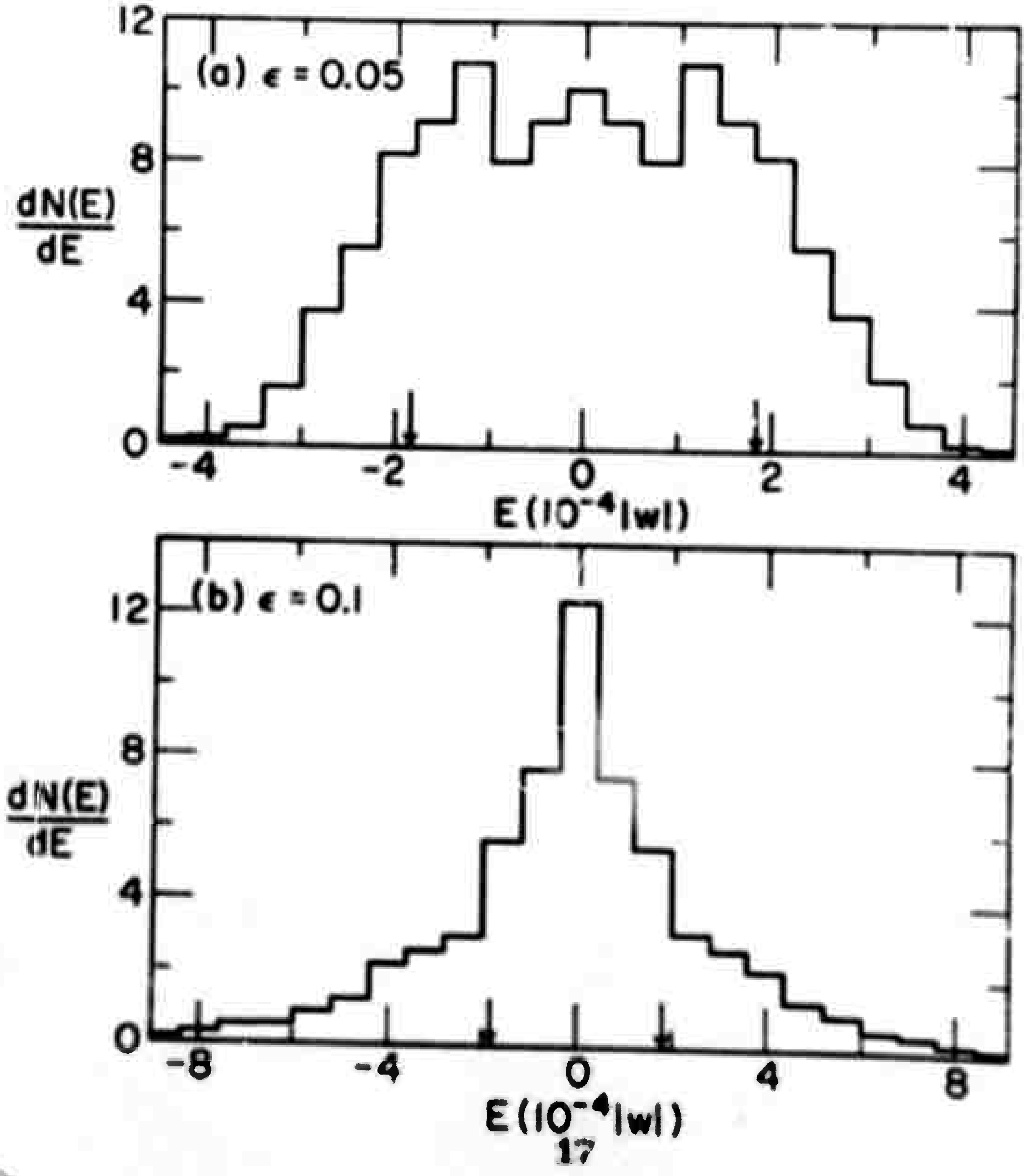

(a) ε = 0.05
dN(E)/dE
12
8
4
0
-4
-2
0
2
4
E(10⁻⁴|w|)
(b) ε = 0.1
dN(E)/dE
12
8
4
0
-8
-4
0
4
8
E(10⁻⁴|w|)

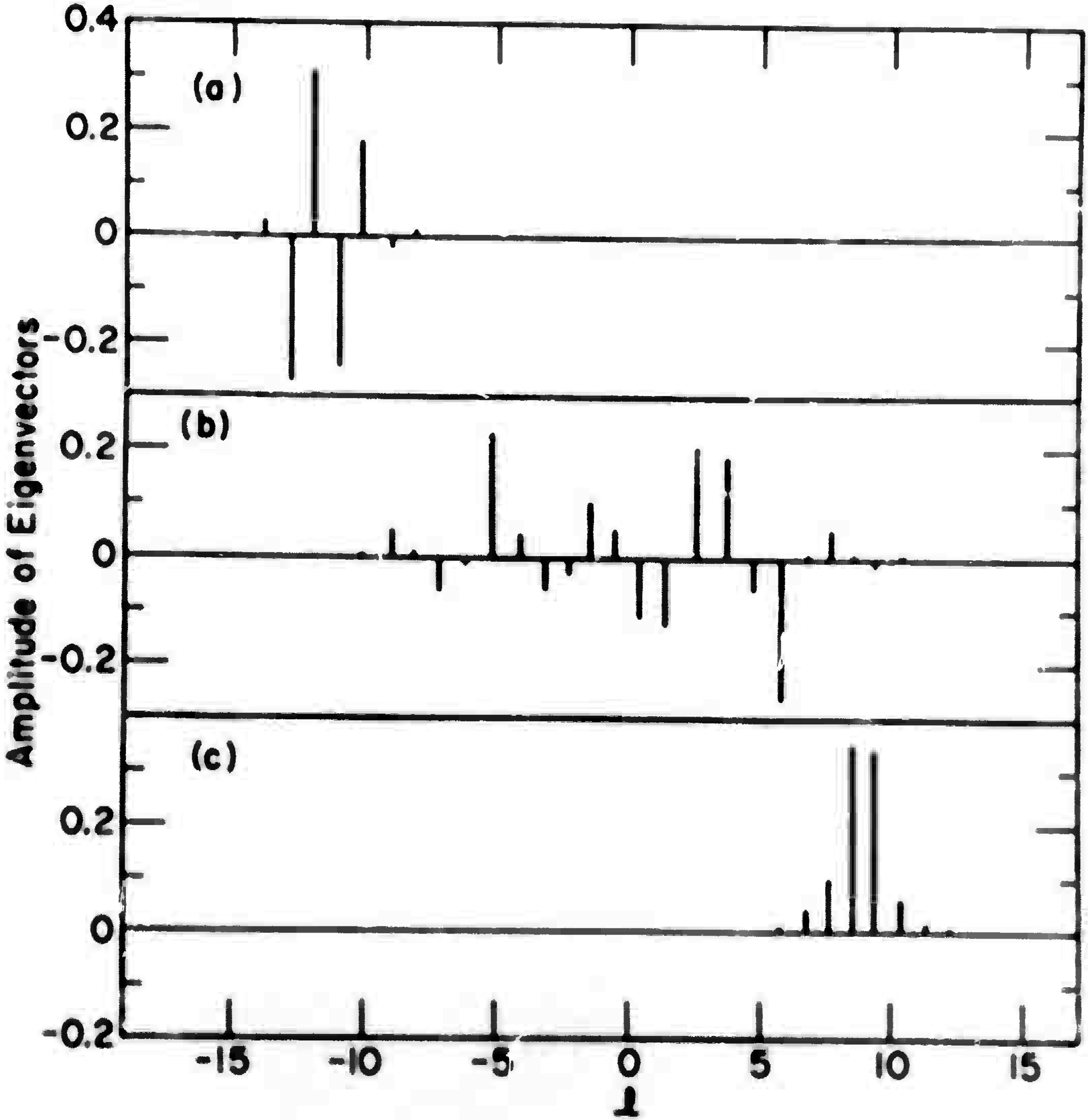
Amplitude of Eigenvectors
(a)
(b)
(c)
0.4
0.2
0
-0.2
-15
-10
-5
0
5
10
15
l

Models for Steady State Electron Injection Current into Dense Media*

P. Smejtek, M. Silver, I. L. Huang and K. S. Dy

University of North Carolina at Chapel Hill

Chapel Hill, North Carolina 27514

Abstract

Two models, the Monte Carlo and the diffusion model for calculating the electron current due to injection of hot electrons into dense media are presented. In the diffusion model, the current can be derived exactly by solving the continuity of current equation numerically assuming a fast energy relaxation two-level system. However a very simple analytic expression for the current is obtained if one uses a strong diffusion approximation for the hot electrons. The validity and errors resulting from the approximation are discussed. When the diffusion model fails, we propose a simplified Monte Carlo model for calculating the current. The model is a modification of an earlier method by Young and Bradbury to include the effect of multiple scattering and the influence of the image potential.

I. Introduction

Electron injection experiments have played a powerful role in determining the electronic transport properties of insulating solids,[1] liquids[2] and gases[3]. However, up until recently, there is still a lack of an adequate theoretical model for explaining the dependence of the experimentally measured current on the applied electric field, the characteristics of the medium, and the electron-medium interaction. Perhaps the first calculation of the current-voltage relation resulting from charge injection was due to J. J. Thomson[4]. Thomson assumed that near the cathode the injected electrons have a random velocity $\bar{v}_0$ given by thermal equilibium with the gas and that the density of electrons in the gas is uniform and of average value n. This implies that there is a back-diffusion current given by $ne\bar{v}_0/4$. In the presence of an applied field, the current will be given by $j=ne\bar{v}$ where $\bar{v}$ is the drift velocity. Thus if j_0 is the total injected current, we get from Thomson's result $j_0-j=ne\bar{v}_0/4$, and

$$j/j_0=4\bar{v}/(\bar{v}_0+4\bar{v}) . \tag{1}$$

Theobald[5] and Loeb[6] found that Eq. (1) gives reasonable fit to experiment only if $\bar{v}_0$ is reinterpreted as the average velocity of emission. Bekierian[7] improved the theory further by taking the back-diffusion current to be $n_p e\bar{v}_0/4$ and the measured current to be $n_\infty e\bar{v}$ where n_p and n_∞ are the densities of electrons near and far from the cathode respectively. The applicability of the theory presented above is quite restricted even in its modified form. Theobald[5] found that there is a large descrepancy between theory and experiment when the emission velocity becomes much less than the drift velocity. In such a case back-diffusion loss decreases and Thomson's result fails. Another situation where Eq. (1) may be expected to fail is when the back-diffusion zone is under the strong influence of the image field produced by the injected electrons. In such a case the return of electrons to the cathode is not given by back-diffusion alone.

Perhaps the correct approach to the solution of the problem would be to do a Monte Carlo calculation including all the fields experienced by the electrons and all the important scattering processes encounter by the electrons. This is a very time consuming calculation. One simplified approach to this was made by Young and Bradbury [8] who calculated the return current assuming only reflection of electrons in their first encounter with gas atoms or molecules. They found that for $j/j_0<0.2$ the current is given by

$$\frac{j}{j_0} \approx \frac{1}{2}\pi^{1/2}\left(\frac{eE\lambda}{\epsilon_0}\right)^{1/2} \tag{2}$$

where λ is the mean free path, E is the applied field and ϵ_0 is the energy of the injected electrons. Unfortunately the validity of Eq. (2) is difficult to access as there is no simple way of estimating the effects of multiple scattering.

In this paper, we shall present two theoretical models for the steady state electron injection currents. The first model is a modification of the Young and Bradbury model to account for the effects of both image field and multiple scattering. The model is applicable to cases where the electron momentum and energy relaxation rates are slow. The second model is a two fluid model in which the electrons are divided into a hot and a thermalized component. The currents are derived by solution of the continuity of currents equation. This model is applicable when the momentum and energy relaxation rates of the electrons are fast.

II. Simplified Monte Carlo Model

In this section we present a simplified Monte Carlo method for calculating the current in an experimental situation depicted in Fig. 1. An electron is injected into the medium with energy ϵ_0. In the medium the electron experiences the total potential $V(x)$ consisting of the image potential $-\frac{e^2}{4\epsilon x}$ and the applied potential

$-eEx$. Let us consider first the case in which the scattering of the electron is elastic. In our simplified model we shall make the following basic assumptions:

(a) The scattering of an electron with a particle in the medium is s-wave.

(b) The direction of motion of the electron after each collision is independent of the previous collision.

(c) The thermal velocity of the scatterers in the medium are negligible.

(d) The trajectories of the electron between collisions are linear and their path lengths s distributed according to $\exp(-s/\lambda)$ where λ is the momentum exchange mean free path.

Assumption (a) can be easily corrected to include other partial waves. Assumption (b) is valid if the average collision duration of an electron with the scattering center is much shorter than the time between collisions. Assumption (c) limits our presentation to mediums with extremely low temperature. In these cases the electron loses its kinetic energy at each collision only through the recoil of the scatterer and the amount lost is simply calculated. This assumption shortens our Monte Carlo calculation considerably but it is by no means necessary. At higher temperatures, one can for examply assign a Maxwell-Boltzmann distribution of velocities to the particles in the medium. The change in kinetic energy of the electron after a collision can then be computed from the collision kinematics. In this paper, we only present the $T=0^{\circ}K$ results.

Assumption (d) is correct if the mean free path of the electrons is so short that between collisions they don't pick up (or lose) enough kinetic energy from the field to deflect their trajectories significantly. In this case the problem reduces to a straight diffusion problem and it can be handled simply for example by solving a Boltzmann aquation treating the field as a perturbation. We shall be interested in cases whare the influence of the image and driving fields are strong so that assumption (d) has to be corrected to take into account trajectories with turning points and the fact that most trajectories will be bent toward the direction of the field. Since such calculations would require a tremendous amount of computer time, we correct for the effect in the following approximate way. Let us consider an electron located at a position x to the right of the potential maximum x_M as shown in Fig. 1. The probability that the electron will be reflected backward by the fields at that point will be proportional to the return cone [8],

$$\Omega(x) = 2\pi\left\{1-\left[\frac{V_M-V(x)}{\varepsilon_0-V(x)}\right]^{1/2}\right\} \tag{3}$$

We shall define a reflection coefficient, r(x) and a transmission coefficient t(x) for an electron at a distance $x>x_M$ from the cathode to be $r(x)=\Omega(x)/4\pi$ and $t(x)=1-r(x)$. For $x<x_M$, r(x) and t(x) simply exchange roles. In our model we assume as in (d) that the trajectories are linear, but correct it approximately by weighting the forward and backward trajectories according to t(x) and r(x) respectively. Thus our simplified Monte Carlo calculation proceeds as follows:

(1) Electrons are injected into the medium with energy ε_0 and with an initial angular distribution $f(\theta_0,\phi_0)$. In the present calculation we take ε_0 to be monoenergetic and $f(\theta_0,\phi_0)$ to be in the forward direction so that the current can be correlated with injection into vacuum where the escape cone is expected to be small.

(2) The length of the trajectory s of a given electron is determined by $-\lambda \ell n r$, where r is a random number between 0 and 1, and λ is the momentum exchange mean free path.

(3) At the end of the trajectory where a collision event has occured, the electron losses approximately $\frac{2m}{M}(1-\cos\theta)$ of its kinetic energy to the recoil of the molecule. m and M are the masses of the electron and the scatterer respectively and θ is the angle between the incident and final velocities of the electron.

(4) After the collision, tha direction of motion of the electron with respect to the x axis is given by $\theta = \cos^{-1} r$ where r is a random number between 0 and 1 . The choice of θ in the forward or backward direction is weighted according to $t(x)$ and $r(x)$ respectively.

(5) Taking the angle of step (4) as the new initial angle we repeat the process of generating the trajectories until the final point where the kinetic energy becomes less than the potential maximum V_M . Then the electron is considered transmitted if its final position x is greater than x_M and returned otherwise.

(6) If in addition thare are inelastic processes in the medium, we need to know all the possible modes of energy transfer and their respective cross-sections. The number of each typa of inalastic events is then generated in direct proportion to their cross sections.

The results for the Monte Carlo calculation of the current as a function of E/N where E is the strength of tha applied field and N is the density of particle in the medium is shown by the solid curve in Fig. 2. In thesa calculations two atomic masses were considered, M=2 and M=40, and only elastic scatterings were included. The scattering cross section was taken to be $10^{-15} cm^2$ and the density 10^{21} atoms per cm^3 . The results are independent of the masses to within the statistical fluctuation due to the finite number of elactrons (10^4) injected. The Young and Bradbury result is shown by the dashed curve. The agreement betweem the Young and Bradbury result and the Monte Carlo result is quite good at high fields for the density and cross-section considered.Under such conditions it is reasonable to neglect the image field and the single scattering approximation is valid because the transmission coefficient rapidly becomes one. At lower fields, the Monte-Carlo results gives lesser end lesser currents compared with the Young and Bradbury results. The differences arise from incluaion of the image field and multiple scattering. The deviation will become smaller if we consider finite temperature cases as part of the current will thermally diffuse across the potential barrier.

III. The Diffusion Model

When there is rapid momentum and energy relaxation it becomes simpler to calculate the current by a diffusion model. First we shall discuss the injection of monoenergetic electrons into the medium where the momentum exchange m.f.p. is λ and the strength of the inelastic electron-medium interaction is given in terms of an average lifetime τ. Because we use only a single relaxation time the system can be characterized by a two-components fluid, i.e. hot electrons, the density of which are given by ρ_h, and the thermalized electrons with ρ_t specifying their density. Because $\nabla\cdot(\vec{j}_h+\vec{j}_t)=0$, we have simply for the case of planar geometry:

$$-\frac{d}{dx}(j_h) - \rho_h/\tau=0 \tag{4}$$

where

$$j_h=-D_h\frac{d\rho_h}{dx} + \mu_h\left(E-\frac{e}{4\epsilon x^2}\right)\rho_h \tag{4a}$$

and

$$-\frac{d}{dx}(j_t)+\frac{\rho_h}{t}=0 \tag{5}$$

where

$$j_t=-D_t\frac{\partial\rho_t}{dx}+\mu_t\left(E-\frac{e}{4\epsilon x^2}\right)\rho_t \tag{5a}$$

In these equations D is the diffusion constant, μ is the mobility and ϵ is the dielectric constant of the medium which we shall set equal to 1. Since Eq. (4) is decoupled from the thermal component we can find its solution independently. One boundary condition is given by the current balance at one scattering m.f.p. from the emitter. One part of the electron current injected is scattered back without appreciable energy loss and is given by the Thomson's term $\rho_h(\lambda)\langle v_x(\lambda)\rangle$. $\langle v_x(\lambda)\rangle$ is the average over all angles of the x component of the velocity at λ in the presence of the applied and image fields. If we define $\langle v_x(\lambda)\rangle \equiv c(\lambda)\bar{v}_0$, where $\bar{v}_0$, is the average emission velocity, then $c(\lambda)$ must approach the Thomson value of 1/4 as λ becomes larger or of the order of x_M , the position of the potential maximum. The details of the calculation of $c(\lambda)$ are shown in appendix 1. Another part of the current at λ is that diffusing into the medium and given by $\int_\lambda^\infty \tau^{-1}\rho_h(x)dx$. Consequently for current balance at λ , the boundary condition is

$$j_0 = c(\lambda)\rho_h(\lambda)\bar{v}_0 + \tau^{-1}\int_\lambda^\infty \rho_h(x)dx \qquad (6)$$

where j_0 is the current supplied by the emitter. Another boundary condition we shall use is

$$j_h(\infty) = 0 \, . \qquad (7)$$

Integrating Eq. (4) from x to ∞ and using (7) gives

$$j_h(x) = \tau^{-1}\int_x^\infty \rho_h(x)dx \qquad (8)$$

We shall show that the measured current j can be derived from $j_h(x)$ alone. We start by discussing the T = 0 K case. At T = 0 K, the diffusion part of the thermal current given by Eq. (5a) vanishes as D_t=0. At x = x_M, the field driven current also vanishes as the field is zero at x_M . Thus $j_t(x_M) = 0$, and the measured current

$$j(T=0) = j_h + j_t = j_h(x_M) \quad . \qquad (9)$$

For finite temperatures, j_t is nonvanishing at x_M and we have to adopt another method. Since $j = j_h(x) + j_t(x)$ we get after substituting Eq. (5a) for j_t and $-\frac{dv}{dx}$ for the total field the following equation,

$$j-j_h(x) = -D_t \frac{d\rho_t}{dx} - \mu_t \frac{dV}{dx}\rho_t$$

Solving this equation for ρ_t we get

$$\rho_t(x) = \exp-[(\mu_t/D_t)V(x)]\int_0^x \frac{j_h(x')-j}{D}\exp[(\mu_t/D_t)V(x')]dx' + \rho_t(0) \qquad (10)$$

As $x\to\infty$, we don't expect ρ_t to diverge, but since $V(x)\to-\infty$, we must require that the integral in Eq. (9) vanishes. Thus we obtain

$$j = \frac{\int_0^\infty j_h(x)\exp[eV(x)/kT]dx}{\int_0^\infty \exp[eV(x)/kT]dx} \qquad (11)$$

where we have made use of the Einstein relation $\mu_t/D_t = \frac{e}{kT}$. We shall use Eq. (9) and Eq. (11) to calculate the current and as mentioned earlier, they depend only on $j_h(x)$.

We now discuss the derivation of $\rho_h(x)$ from which $j_h(x)$ can be calculated. Substituting Eq. (4a) into Eq. (4), we get

$$D_h\frac{d^2\rho_h}{dx^2} - \mu_h(E - \frac{e}{4\epsilon x^2})\frac{d\rho_h}{dx} - (\frac{\mu_h e}{2\epsilon x^3} + \frac{1}{\tau})\rho_h = 0 \qquad (12)$$

Equation (12) can be solved exactly by numerical method. Typical solutions are shown in Fig. 3. Here we shall present a simple approximate solution and discuss its validity. We note that if the terms in Eq. (12) arising from the image field can be neglected, then the remaining equation can be solved analytically. We expect that the approximation might be justified for x above a certain distance x_{SD} for which $-D_h\frac{d\rho_h}{dx} \gg \mu_h \frac{e}{4\epsilon x^2}\rho_h$, and we call this the strong diffusion approximation (SDA). Estimates of x_{SD} are given in detail in appendix 2. The SDA solution to

Eq. (12) is simply

$$\rho_h(x) = \rho_h(\lambda)\, e^{-\gamma(x-\lambda)} \tag{13}$$

where

$$\gamma \equiv -\frac{\mu_h E}{2D_h} + \left[\left(\frac{\mu_h E}{2D_h}\right)^2 + x_0^{-2}\right]^{1/2} \tag{14}$$

and
$$x_0^{\,2} = D_h \tau \tag{15}$$

Applying the boundary condition (6), and $D_h = \frac{1}{3}\lambda\bar{v}_0$, we find

$$\rho_h(\lambda) = \frac{j_0}{\bar{v}_0}\left[C(\lambda) + \frac{\lambda}{3\gamma x_0^{\,2}}\right]^{-1} \tag{16}$$

The comparisons of the SDA solution with the exact solution are shown in Fig. 3. It is observed that the deviation is greater for electrons of lower energy and shorter mean free path. This deviation is to be expected since under these conditions the diffusing electrons are more exposed to the influence of the image field. Their random velocity becomes also more sensitive to the change in the potential energy and the electrons undergo more scattering events closer to the emitter where the retarding field is high.

We can now calculate the SDA expression for the current by substituting (13) into (8) and then use (9) or (11). We shall discuss here the T=0K case only as the following simple analytic expression for j follows from (9),

$$\frac{j}{j_0} = \frac{\lambda}{3\gamma x_0^{\,2}}\left[C(\lambda) + \frac{\lambda}{3\gamma x_0^{\,2}}\right]^{-1} e^{-\gamma(x_M-\lambda)} \tag{17}$$

A typical current versus E/N curve is shown by the solid curve in Fig. 4. For illustrative purposes we choose the medium to be nitrogen with a density of

10^{22} molecules /cm^3. We assume an inelastic process in which an electron loses 0.25 eV at each collision with a cross section of 10^{-18} cm^2, and we take the momentum exchange cross section to be 3×10^{-16} cm^2. The electrons are injected with energy ϵ_0 =1eV. The field dependence of the current enters through $x_M = (e/4\epsilon E)^{1/2}$. By changing the applied field the potential maximum can be shifted, in this way the image barrier probes the spatial distribution of the hot electrons. At low fields, x_M is large and a large portion of the hot electrons relaxed before reaching the potential maximum. This gives rise to an exponential drop in the current given by

$$\frac{j}{j_0} \approx e^{-x_M/x_0}(\lambda/3x_0)/(C+\frac{\lambda}{3x_0}) \tag{18}$$

At large fields, γ becomes quite small $\gamma \approx D_h/\mu_h E x_0{}^2$ and

$$\frac{j}{j_0} \approx \frac{\frac{\lambda\mu_h E}{3D_h}}{c(\lambda)+\frac{\lambda\mu E}{3D_h}} = \frac{\bar{v}}{c(\lambda)\bar{v}_0+\bar{v}} \tag{19}$$

which is simply Eq. (1), the prediction of Theobald[5] and Loeb[6]. It is interesting to notice that in the high fields limit, the diffusion model predicts that the current is independent of the inelastic processes. The reason is that most electrons are relaxing beyond the potential maximum in this limit.

We have also investigated what would happen if the diffusion model were not applicable and the Monte Carlo model have to be used. The results are presented in Fig. 4. In the high field region (shown by dots) agreement in the order of magnitude of the current can be achieved only by using $\sigma_p = 4\text{x}10^{-16}$cm^2 and $\sigma_i = 10^{-18}$cm^2. The insensitivity to the inelastic processes is preserved, but the field dependence has clearly gone over to the $E^{1/2}$ behavior. In the low field region (shown by triangles) the overall field dependence can be fitted quite well with $\sigma_p = 1.9 \times 10^{-16}$ cm^2 and $\sigma_i = 2 \times 10^{-18}$ cm^2. The discrepancies in this region are due on one hand to the fact to be shown later that the SDA underestimates m.f.p. and overestimates lifetimes. On the other hand the Monte Carlo model does exactly the opposite by overestimating the return current because the return trajectories are approximated by straight paths. Evidently weighting the return trajectories by their reflection coefficients presents only a partial correction to the actual curved paths. Actually the diffusion model and the Monte Carlo model presented here have quite different applicability. We applied it to the same condition here to show the discrepancies one might expect.

Most of our discussions in this section are based on the SDA assumption. As mentioned earlier, the exact solution to the continuity of current equation can be obtained numerically. It is of interest to estimate the error in the electron m.f.p. and hot electron lifetime if one uses the SDA model. The estimates are presented in detail in appendix (3). We find that the SDA model underestimates electron m.f.p. and overestimates lifetime. For electron energy around 1 eV the error is quite small, however, for electron energy below 0.1eV and electron m.f.p. of the order of 10 Å the error may exceed a factor of 2. In an experiment, the electrons are usually injected with a certain energy distribution. In appendix (4), the dependence of the measured m.f.p. and lifetime on the energy distribution of the injected electrons is discussed. The studied distributions of injected electrons are (a) monoenergetic, (b) photoelectric and (c) thermionic. The thermionic distribution is of special interest since a larger amount of the emitted electrons have lower energies. Because of this feature the SDA indicates in this case a greater error than the other two distributions. For the average injection energy of 1 eV and 20 Å m.f.p. the error is about 30% for the thermionic, about 10% for the photo electric and 15% for the monoenergetic distribution.

IV. Conclusion

In summary, we have presented two models, the Monte Carlo model and the diffusion model for calculating the electron injection current into dense media. The diffusion model applies if the kinetic energy gained from the field by the electron between collisions is small so that it is possible to decompose the current into a diffusing component and a drift component. The resulting current can be derived exactly by solving the continuity of current equation numerically. However, a very simple analytic expression for the current is obtained in the strong diffusion approximation (SDA). For [illegible] and high fields the SDA result reduces to that derived by Theobald (5) and Lamb (6). When the diffusion condition fails, the field dependence approaches $\sim \mathcal{E}^{1/2}$. This dependence was predicted by Young and Bradbury (4) with a single-scattering - Monte-Carlo calculation. In this paper we extended the Young and Bradbury method to include multiple scattering and the effects of the image field. Important deviations occur at low fields where the return zone is strongly influenced by the image potential.

Both the models we have presented are very simple to use. They are complimentary and can be applied to a wide range of experimental situations. Some of these applications will be discussed in the following paper.

*Work supported by the U. S. Army Research Office (Durham) and by the Advanced Research Projects Agency of the Department of Defense and monitored by the U. S. Army Research Office - Durham under Grant number DA-ARO-D-31-124-71-G32.

References

(1) M. A. Lampert, P. Mark, Current Injection in Solids, Academic Press, 1970.

(2) R. Schnyders, S. A. Rice, L. Meyer, Phys. Rev. 150, 127 (1966); B. Halpern, R. Gomer, J. Chem. Phys. 51, 1031, (1969); R. A. Holroyd, M. Allen, J. Chem. Phys. 54, 5014 (1971).

(3) A. V. Phelps, Rev. Mod. Phys. 40, 399 (1968).

(4) J. J. Thomson, G. P. Thomson, Conduction of Electricity Through Gases, p. 444, Cambridge, 1928.

(5) J. K. Theobald, J. Appl. Phys. 24, 123 (1953).

(6) L. B. Loeb, Basic Processes of Gaseous Electronics, p. 601, University of California Press, 1955.

(7) A. [illegible], J. de Physique 23, 436 (1962).

(8) L. A. Young, N. E. Bradbury, Phys. Rev. 43, 34 (1933).

Appendix 1.

In order to calculate the rate of back scattered electrons, Thomson assumed that only those electrons at a distance of one m.f.p. from the electrode were collected. Further he assumed that because of scattering the angular distribution of these electrons was isotropic. In the absence of any electric field, the time of flight of an electron scattered at an angle θ with the $-x$ axis was $\lambda/v_0\cos\theta$. The average x component of the velocity is given by

$$\langle v_x \rangle = \frac{v_0}{2}\int_0^{\pi/2} \cos\theta \sin\theta d\theta = \frac{v_0}{4} \qquad \text{(A1)}$$

In our calculations we have included the effect of the image and the applied field upon the magnitude and direction of the velocity of the electrons as it goes from λ to the electrode. From simple energy conservation

$$v_x(\lambda) = v_0[1+(e^2/4\epsilon\lambda\epsilon_0)+eE\lambda/\epsilon_0]^{1/2}\cos\theta \qquad \text{(A2)}$$

where ϵ_0 is the injection energy (see Fig. 1).

Now

$$-\frac{dx}{dt} = v_x(x) = (v_x^2(\lambda)+v_0^2(e^2/4\epsilon\epsilon_0)[(1/x)-(1/\lambda)]+v_0^2 eE/\epsilon_0(\lambda-x))^{1/2} \qquad \text{(A3)}$$

from which we can calculate the time of flight which is

$$t(\theta) = v_0^{-1}\int_0^{\lambda}((1+\frac{e^2}{4\epsilon\lambda\epsilon_0})\cos^2\theta+\frac{e^2}{4\epsilon\epsilon_0}(\frac{1}{x}-\frac{1}{\lambda}))^{-1/2}dx \qquad \text{(A4)}$$

In Eq. (A4) we have neglected the small effect of the applied field. The average velocity then is

$$\langle -v_x(\lambda)\rangle = \frac{\lambda}{2}\int_0^{\pi/2} \frac{\sin\theta\, d\theta}{\ell(\theta)}\, c(\lambda)\, v_0 \tag{A5}$$

$c(\lambda)$ can be calculated by substituting (A4) into (A5), its values are shown in Fig. (5). For very large λ, $c(\lambda)$ approaches 1/4 as expected.

Appendix II.

In order to estimate the value of x_{SD} such that for $x > x_{SD}$

$$-D_h \frac{dp_h}{dx} \gg \mu_h \frac{e}{4\epsilon x^2}\, p_h \tag{A6}$$

we make the following approximations,

$$\frac{dp_h}{dx} \approx \frac{p_h}{x_0} \tag{A7}$$

and

$$\frac{\mu_h}{D_h} \approx \frac{e^2}{\langle\epsilon\rangle} \tag{A8}$$

where $\langle\epsilon\rangle$ is the average kinetic energy of the electrons, i.e. $\langle\epsilon\rangle = \epsilon_0 + e^2/4\epsilon x$. Substituting (A7) and (A8) into (A6) we find that the inequality (A6) is satisfied for

$$x > [(1+\frac{16\epsilon\epsilon_0}{e^2}x_0)^{1/2}-1]/(8\epsilon\epsilon_0/e^2). \tag{A9}$$

Assuming the thermalization distance $x_o = 100$ Å, we find the critical distance x_{SD} to be 17 Å and 29 Å for 1eV and 0.3 eV electrons respectively. The curves in Fig. 3 shows that the SDA solution and the exact solution agree beyond a critical value of x slightly larger than that estimated here.

Appendix III.

In order to estimate the error in the electron scattering m.f.p. and the hot electron lifetime derived from the SDA, we make the following gedanken experiment. We will inject monoenergetic electron current j_o into a medium at T=OK and measure the collected current which is determined by the value of the current at x_M. This current can be calculated by solving numerically Eq. (12) for assumed values of the actual hot electron m.f.p. λ_{ACT} and lifetime τ_{ACT}. We then analyze the same current using the SDA solution (17), and find λ_{SDA} and τ_{SDA}. The results are shown in Fig. 6 where two cases, (a) ϵ_0 = 1eV and (b) ϵ_0 = 0.3 eV are shown. The m.f.p. and lifetime assumed are labeled λ_{ACT} and τ_{ACT} and those obtained from SDA approximation are λ_{SDA} and τ_{SDA}, respectively. As clearly shown the SDA underestimates λ and overestimates τ. The deviation is larger for lower injection energy and smaller m.f.p.

Appendix IV.

In terms of the strong diffusion approximation at T = OK, the measured current does not depend explicitly on the energy of the injected electrons. If the thermalization distance itself was energy independent, the energy distribution of electrons at the barrier maximum would be identical with the injected one. It would then be possible to correct for the effect of the energy distribution on the error in m.f.p. and lifetime by weighting each with the energy distribution function. However, the assumption of equal relaxation for electrons of different energies is not realistic. It is rather more reasonable to assign equal lifetime to all electrons. This way the relaxation distance becomes energy dependent according to the definition,

$$x_0 \equiv [(2\epsilon_0/m)^{1/2}(\lambda\tau/3)]^{1/2} \tag{A10}$$

In the constant lifetime approximation, the low energy electrons have shorter thermalization distance. The low energy electrons are more strongly attenuated, and therefore, their contribution to the measured current will be less. Another energy dependent effect comes in when we introduce the image potential. Fig. 3 shows that the hot electron density decrease faster in the exact solution than in the SDA solution. Thus the image barrier also distorts the energy distribution of current at x_M. The two effects mentioned above were included in the estimate of errors produced by using the strong diffusion approximation. The error was estimated from the following procedure. For a selected value of the electron m.f.p. and for an assumed energy distribution of injected electrons, a numerical solution of the exact differential equation was sought. From the solution for each energy a contribution to the hot electron current is calculated using Eq. (8). The total current is then found by averaging over all incident energies ϵ_0 according to the energy distribution. For comparison we also analyzed the current by the SDA method where the energy distribution of injected electrons is replaced by a monoenergetic one with ϵ_0 equal to the average energy of the different distribution studied. The resulting discrepancies in λ are shown in Fig. 7a, b, and c. In Fig. 7a the error derived from the exact solution and the SDA are shown for the monoenergetic case. The result will serve as a standard for evaluating the error in λ when the injection energy is not monoenergetic. In Fig. 7b, the assumed distribution is photoelectric with $\frac{dn}{d\epsilon} = (\pi/\epsilon_{max})^2\ \epsilon \sin(\pi\epsilon/\epsilon_{max})$, where

$\epsilon_{max} = \epsilon_{av.}\pi^2/(\pi^2-4)$. In Fig. 7c, the distribution is thermionic with

$\frac{dn}{d\epsilon} = \exp(-\epsilon/\epsilon_{AV})$.

Figure Captions

Fig. 1 Schematic representation of electron injection into a medium. Due to the applied electric field and polarization of the emitter the electron potential energy has a maximum at a distance $x_m = (\frac{e}{4\epsilon E})^{1/2}$

Fig. 2 Comparison between results of Monte Carlo calculations and the simplified theory of Young and Bradbury. The ratio of the collected to the injected current j/j_0 as a function of the ratio of the applied field to number density N. The parameters are $\delta = 10^{-15}cm^2$ and $N = 10^{21}cm^{-3}$.

Fig. 3 Distribution of hot electrons are obtained from the numerical solution to Eq. 12 (solid line) and from the strong diffusion approximation (broken line) for different electron m.f.p.: 1)5Å, 2)10Å, 3)20Å, 4)40Å, and for the energy of injected electrons a) lev; b)0.3 eV.

Fig. 4 Comparison between the analytical solution obtained from the strong diffusion approximation (solid line) and results of Monto Carlo calculations. j/j_0 is the ratio of the collected to the injected electron current, E/N is the ratio of the applied electric field to number density of the medium. Parameters: strong diffusion approximation $\sigma_p = 3\times10^{-16}cm^2$, $\sigma_i = 10^{-18}cm^2$; Monte Carlo: triangles, $\sigma_p = 1.9\times10^{-16}cm^2$, $\sigma_i = 2\times10^{-18}cm^2$; circles, $\sigma_p = 4\times10^{-16}cm^2$, $\sigma_i = 10^{-18}cm^2$. Temperature OK, $N = 10^{22}$ molecules/cm^3.

Fig. 5 Backscattering coefficient $c(\lambda)$ of hot electrons in the image field as calculated from Eq. (A 4) and (A 5) as a function of the electron m.f.p. λ and energy of injected electrons ϵ_0.

Fig. 6 Evaluation of errors produced by application of the strong diffusion approximation to the analysis of the measured current at T=OK. λ_{ACT} and τ_{ACT} are real values of the hot electron m.f.p. and lifetime. λ_{SDA} and τ_{SDA} are the corresponding quantities as determined from the strong diffusion approximation for energy of injected electrons a) ε_0 = 1eV, b) ε_0 = 0.3 eV.

Fig. 7 Evaluation of errors produced by applying SDA method to the analysis of collected current when the distribution of injected electrons is a) mono-energetic b) photoelectric, and c) thermionic.

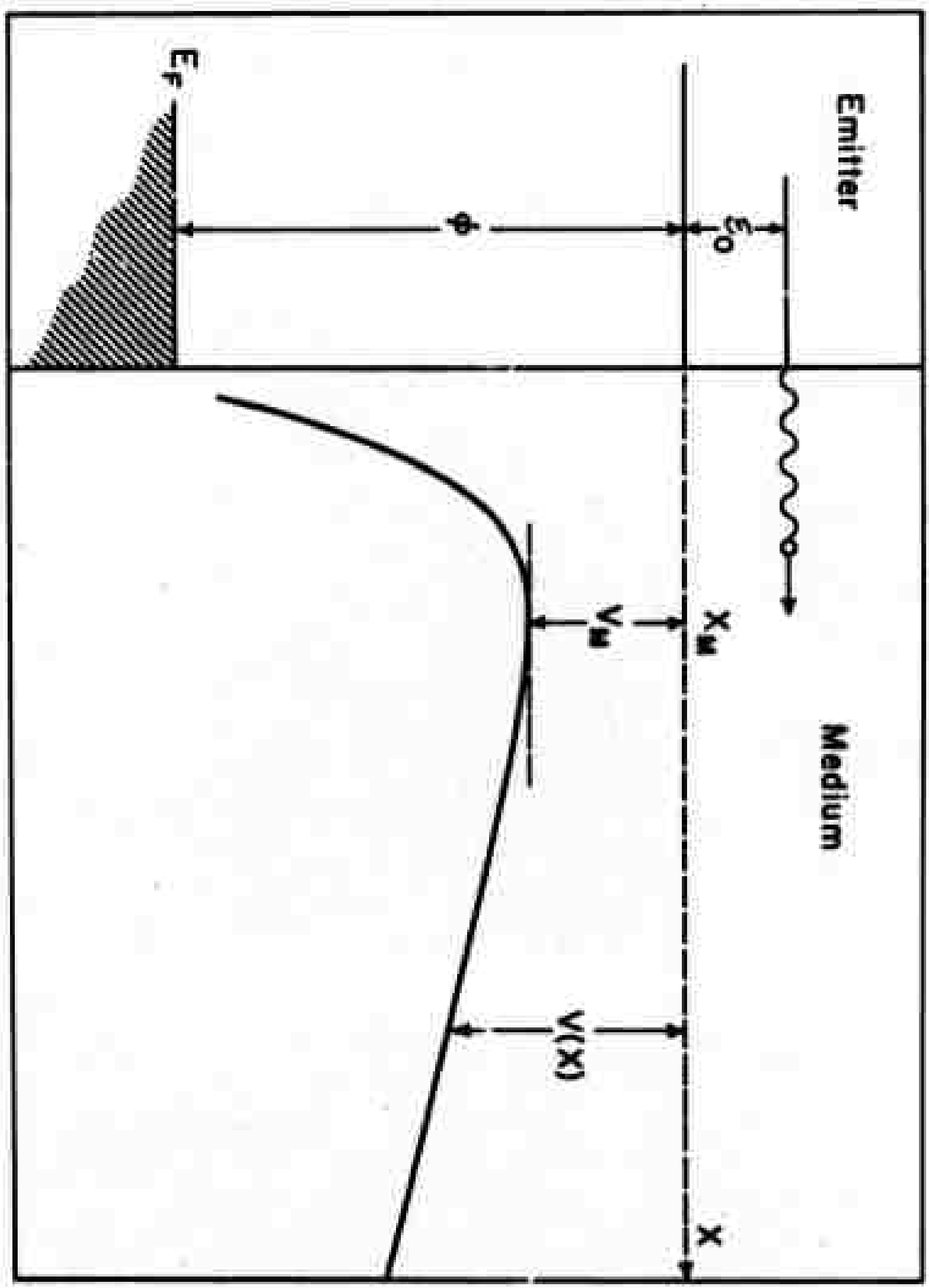

Emitter
Medium
E_F
ϕ
ε_0
X_M
V_M
$V(X)$
X

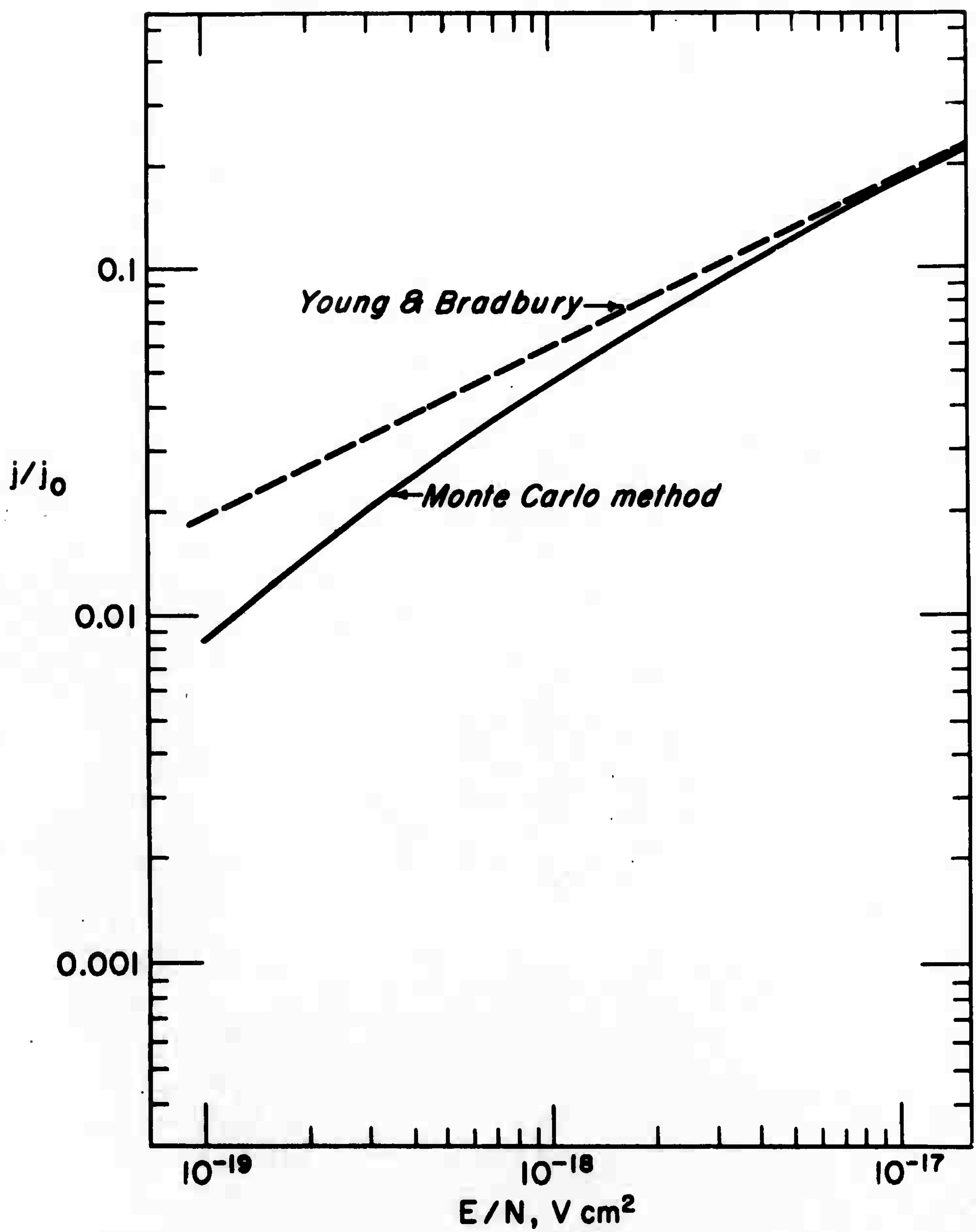

0.1
0.01
0.001
j/j0
Young & Bradbury
Monte Carlo method
10^-19
10^-18
10^-17
E/N, V cm²

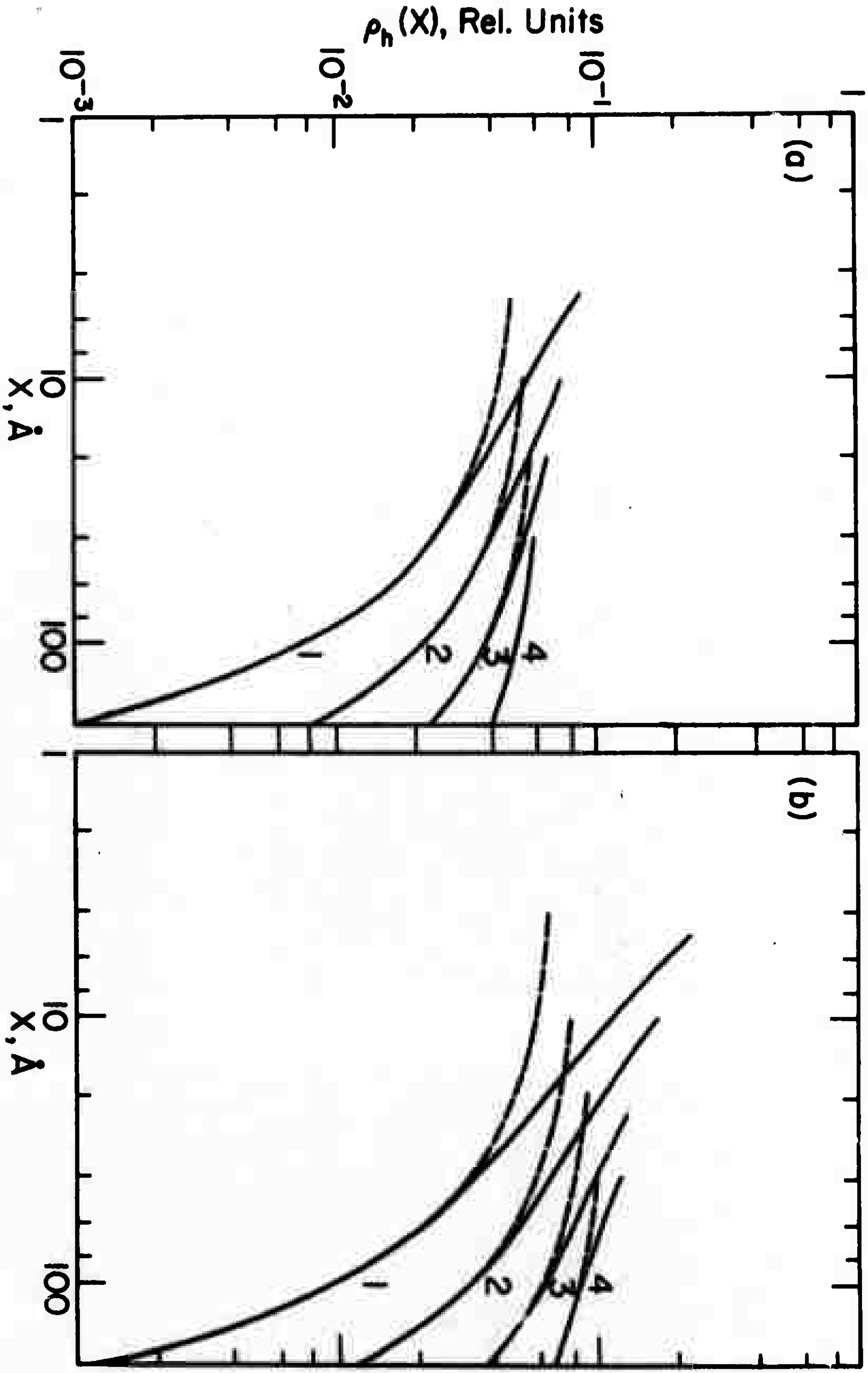

ρh(X), Rel. Units
10⁻³
10⁻²
10⁻¹
(a)
(b)
X, Å
10
100
1
2
3
4

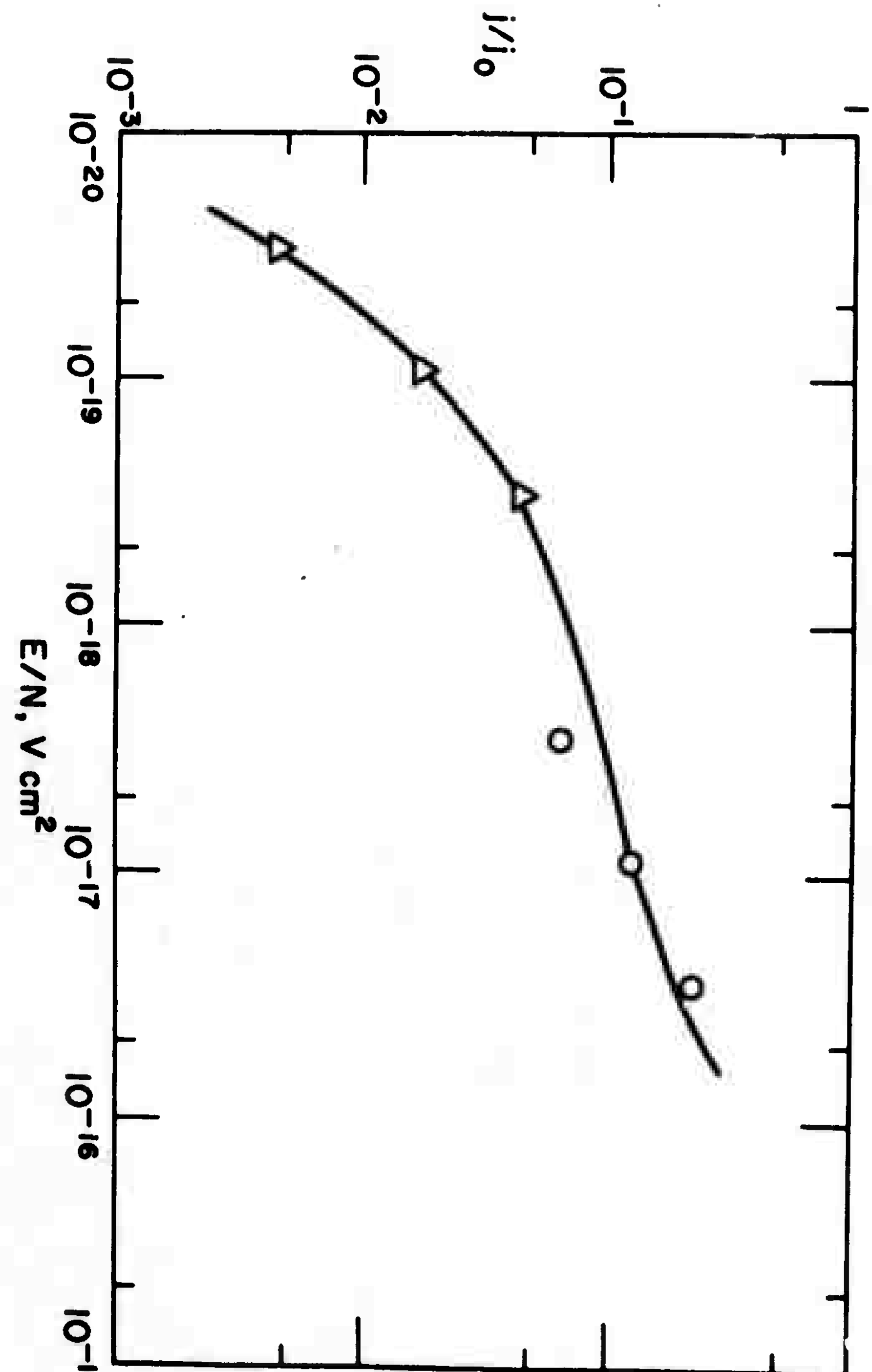

i/i_0
1
10^{-1}
10^{-2}
10^{-3}
10^{-20}
10^{-19}
10^{-18}
10^{-17}
10^{-16}
10^{-15}
E/N, V cm^2

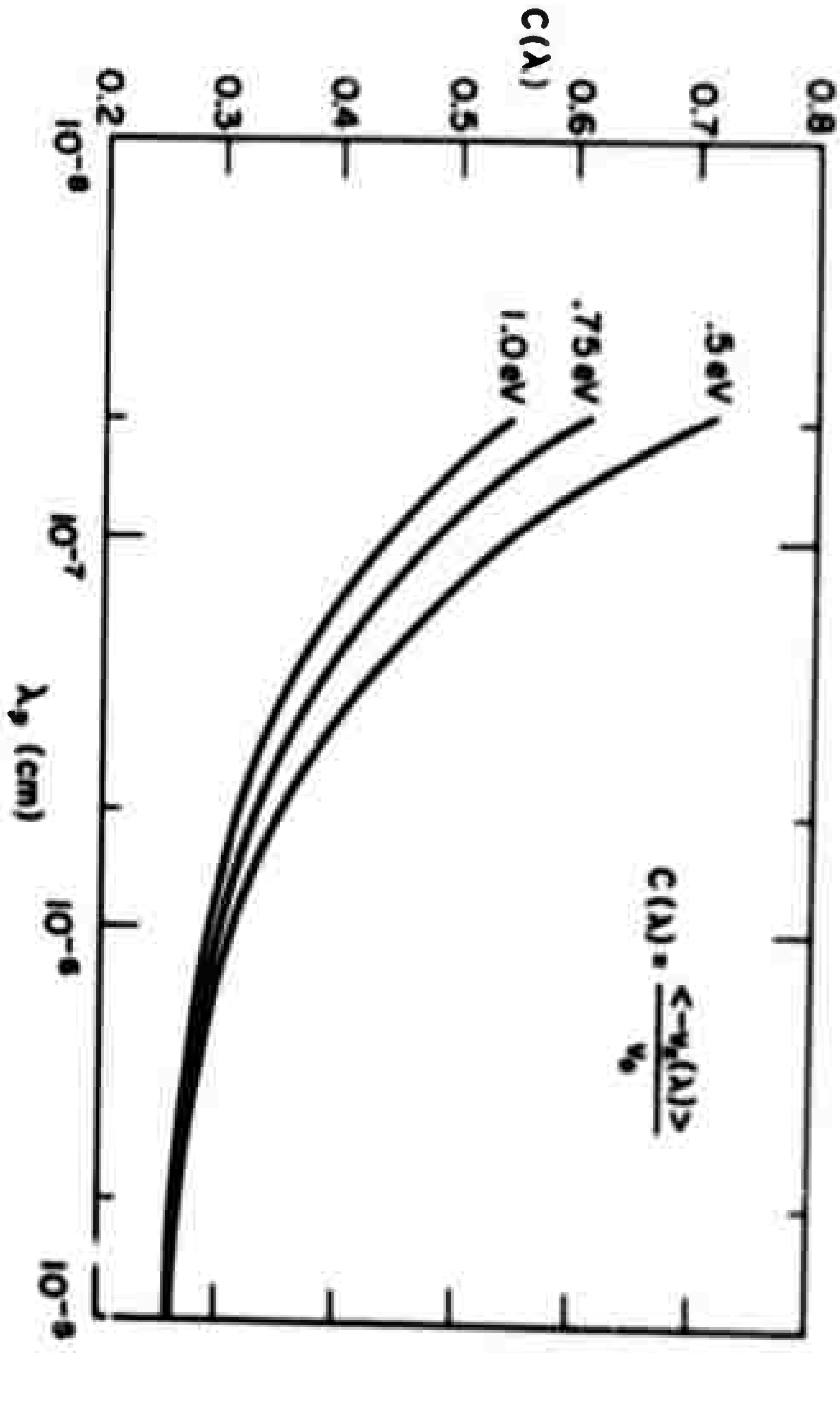
C(λ)
0.2
0.3
0.4
0.5
0.6
0.7
0.8
.5eV
.75eV
1.0eV
10^-8
10^-7
10^-6
10^-5
(cm)

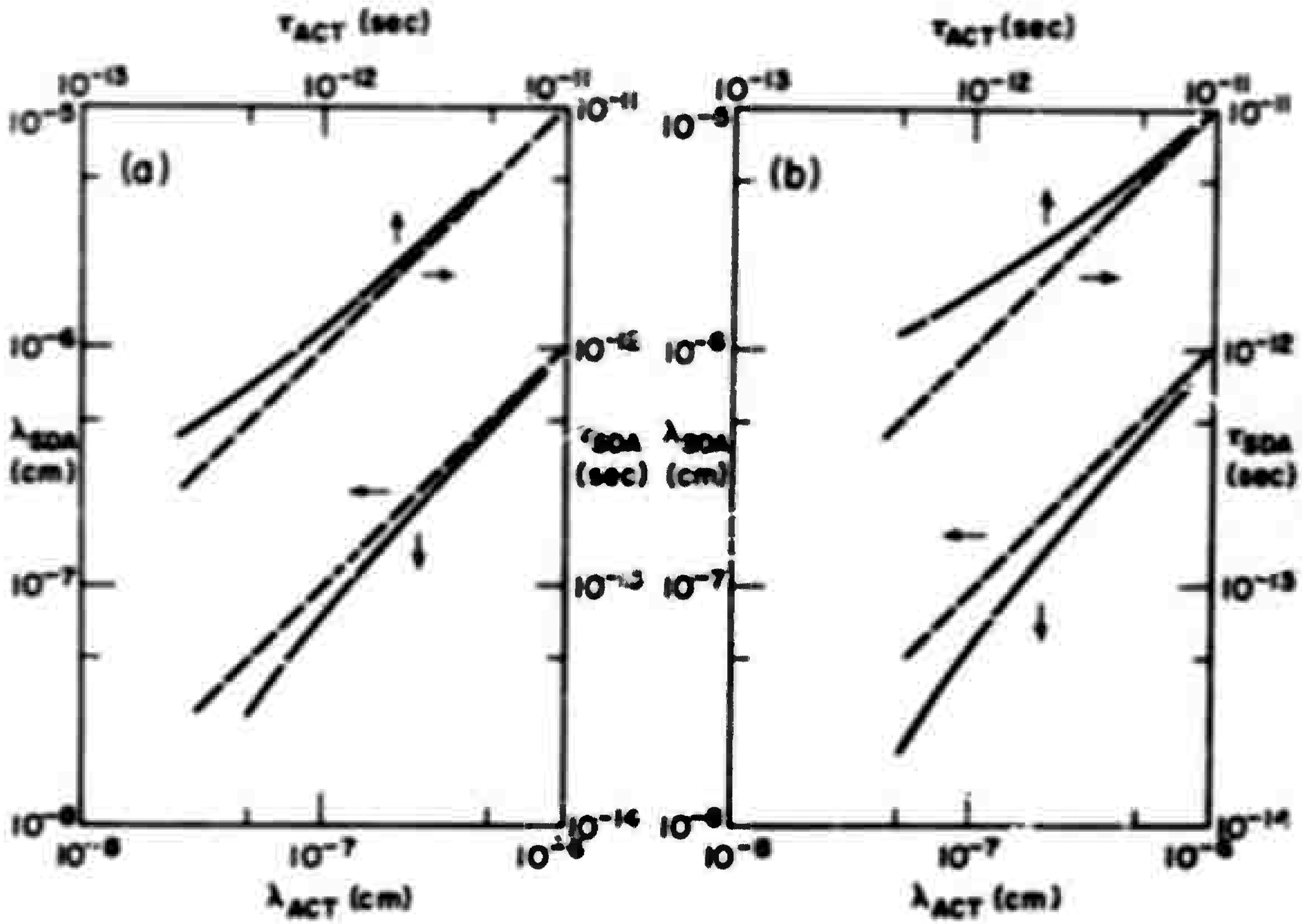

(a)
(b)
τ_{ACT} (sec)
10^{-13}
10^{-12}
10^{-11}
λ_{SDA} (cm)
τ_{SDA} (sec)
10^{-5}
10^{-6}
10^{-7}
10^{-8}
10^{-14}
λ_{ACT} (cm)

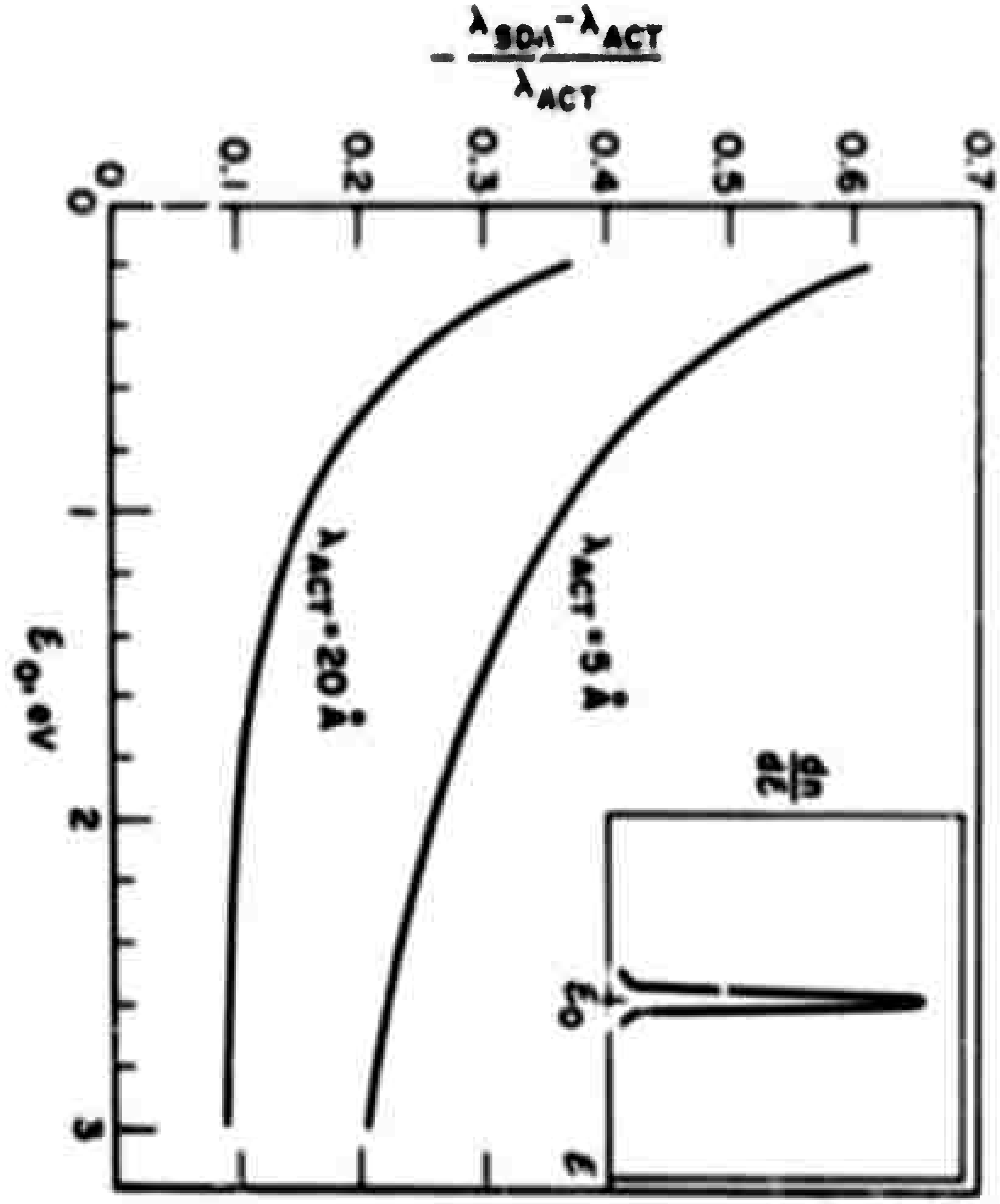

$-\frac{\lambda_{SOA}-\lambda_{ACT}}{\lambda_{ACT}}$
0
0.1
0.2
0.3
0.4
0.5
0.6
0.7
E_0, eV
0
1
2
3
$\lambda_{ACT} = 20$ Å
$\lambda_{ACT} = 5$ Å
$\frac{dn}{dE}$
E_0
E

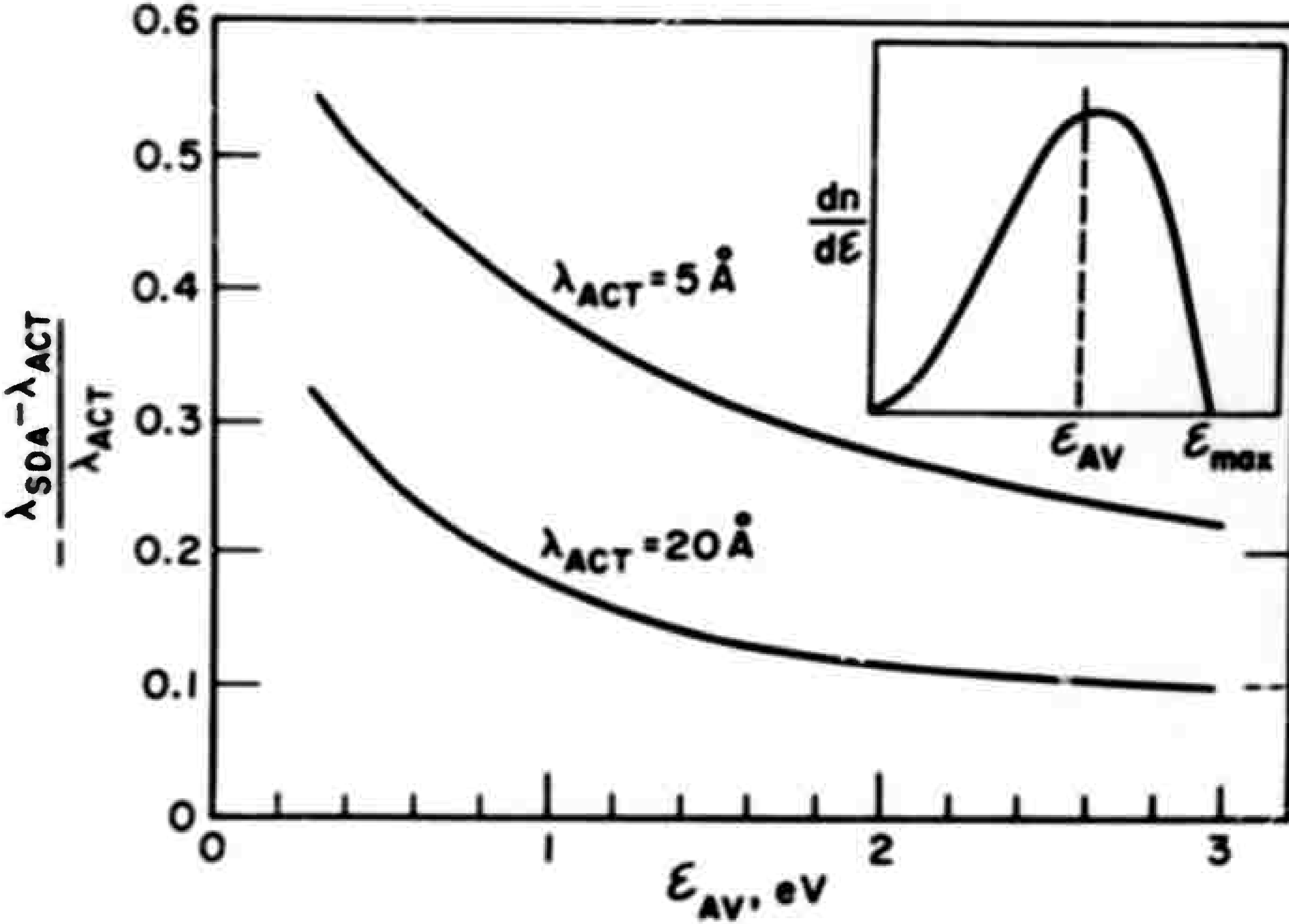

$\frac{\lambda_{SDA}-\lambda_{ACT}}{\lambda_{ACT}}$
0.6
0.5
0.4
0.3
0.2
0.1
0
$\lambda_{ACT}=5$ Å
$\lambda_{ACT}=20$ Å
$\frac{dn}{d\mathcal{E}}$
$\mathcal{E}_{AV}$
$\mathcal{E}_{max}$
0
1
2
3
$\mathcal{E}_{AV}$, eV

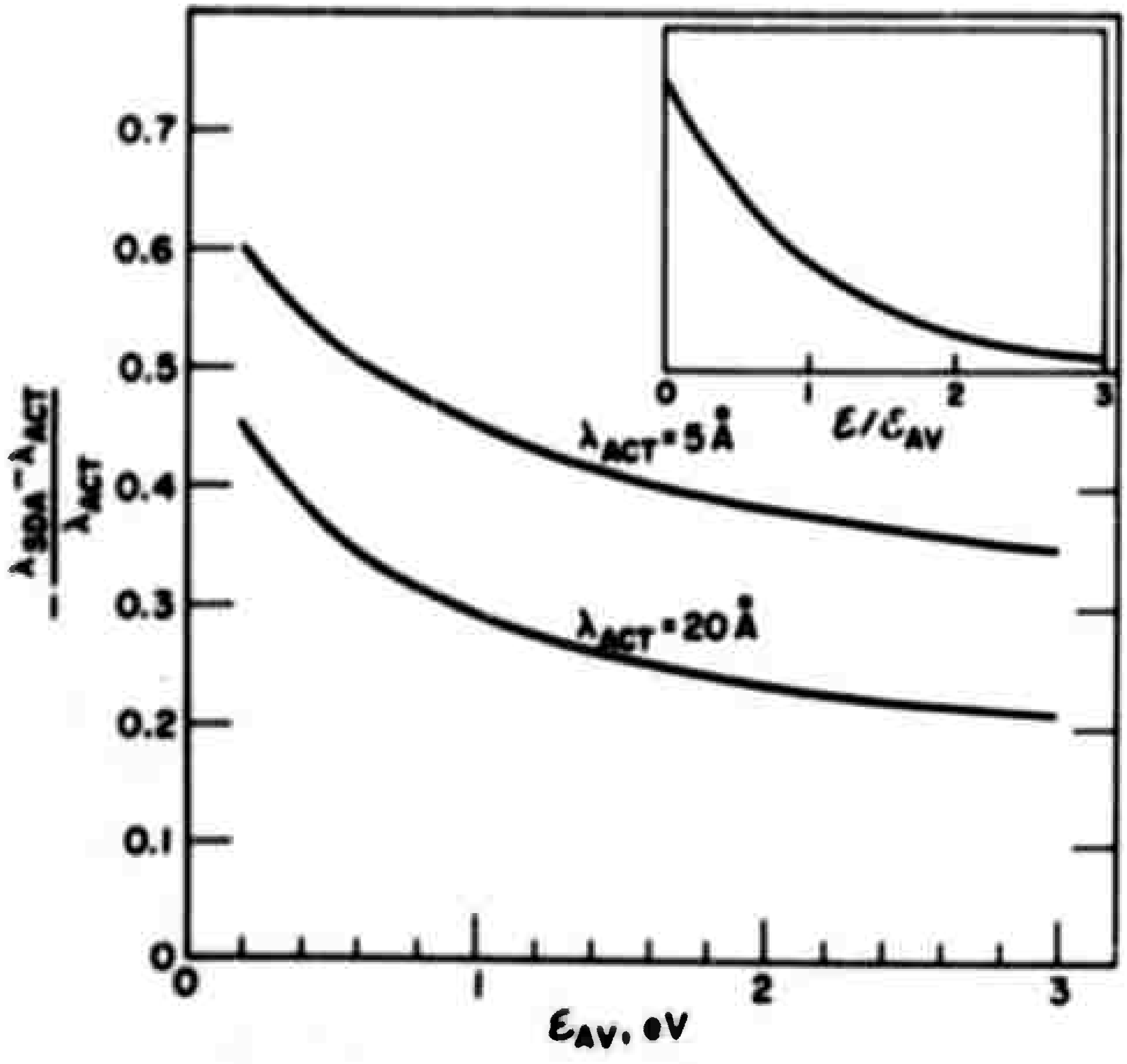
0.7
0.6
0.5
0.4
0.3
0.2
0.1
0
0
1
2
3
$\mathcal{E}_{AV}$, eV
$\frac{\lambda_{30\text{Å}} - \lambda_{ACT}}{\lambda_{ACT}}$
$\lambda_{ACT} = 5$ Å
$\lambda_{ACT} = 20$ Å
$\mathcal{E}/\mathcal{E}_{AV}$

Mobility of Electrons in Dense Helium Gas*

James A. Jahnke and M. Silver

Department of Physics, University of North Carolina

Chapel Hill, North Carolina 27514

We have extended the range of electron mobility measurements in dense helium gas at 77.3 K to pressures of 40 atm and at 160 K to 80 atm. Coexisting high and low mobility branches were found at both temperatures, corresponding, we believe, to free electron and "bubble" states.

The behavior of electrons in dense helium gas serves as an experimental model for the study of electrons in structurally disordered systems.[1,2] A rapid drop in electron mobility as a function of density was suggested by Levine and Sanders[3] to correspond to a self-trapped "bubble" state. Recently their experimental work was extended by Harrison and Springett[4,5] to temperatures above the helium critical temperature (7 K - 18 K) showing

---

* Research supported by the Advanced Research Projects Agency of the Department of Defense and monitored by the U. S. Army Research Office - Durham, under Grant No. DA-AROD-31-124-72-G80, and by the Materials Research Center, U.N.C. under Contract DAHC 15-67-C-0223 with the Advanced Research Projects Agency.

similar rapid decreases in mobility as a function of fluid density. In contrast to the self-trapped model, Eggerter and Cohen interpreted this data in terms of fluctuation trapping in their "pseudobubble" model. Due to the importance of distinguishing between the forms of electron trapping in these theoretical models,[1,3,6] it was felt necessary to extend the mobility measurements even further as functions of temperature and pressure.

Mobilities are determined from the measured electron drift velocity v_d. The zero field electron mobility μ_0 is defined as $\mu_0 = \lim_{E \to 0} v_d/E$ where E is the electric field strength. The drift velocity was measured, in the present experiments, by use of a double gate time-of-flight technique.[7] A thin film $Al\text{-}Al_2O_3\text{-}Au$ diode[8,9] was used as a source of relatively low energy electrons (1 eV at injection); currents of about 10^{-13} to 10^{-11} amps being successfully measured in the present apparatus. Measurements were made as a function of pressure at 77.3 K and 160.1 K by immersing the experimental high pressure cell in dewars of liquid nitrogen and frozen ethanol. Helium gas of 99.95% purity was passed through a liquid-nitrogen-cooled charcoal trap and pressurized. Gas of 99.9995% was also used without any noticeable discrepancies between the measured drift velocities. Pressures were determined using a Heise gauge and temperatures were monitored with a calibrated copper-constantan thermocouple.[7] The gas number densities were calculated from an empirical equation of state,[10] errors estimated as being no greater than $\pm.02 \times 10^{21}$ cm^{-3} at 77.3 K and $\pm.04 \times 10^{21}$ cm^{-3} at 160.1 K. Drift velocity measurements were taken at electric field strengths of 75 V/cm to 200 V/cm at 77.3 K, but only at 100 V/cm at 160.1 K since the field dependent data at the lower temperature appeared linear in this range for densities greater than 1.0×10^{21} cm^{-3} (Fig. 1). Each point on the drift velocity curves is the average of over 12 experimental traces from the spectrometer. Over six harmonics were scanned in some instances for a given point, whereas no less than two harmonics were measured for any given point. The precision of each averaged drift velocity is about 5% and the absolute accuracy of the extrapolated zero field mobilities is estimated to be on the order of 10%.

The zero field mobility results of the present experiments are summarized in Fig. 2 where they are also compared with the recent data of Harrison and Springett for both helium and hydrogen.[4,5] As can be seen, our data at 77.3 K essentially reproduces the earlier data over the range at which it was taken. Also, the existence of two mobility branches is similar to that previously observed in hydrogen. The mobility branches, we observed, coexist over a density range of about .7 x 10^{21} cm^{-3} at both 77.3 K and 160.1 K. The relative amplitudes of the drift velocity peaks were clearly density dependent, with the amplitudes of the high mobility data decreasing with increasing density and the amplitues of the low mobility branch correspondingly increasing. The amplitudes of each branch, at constant density, were normalized to one for a number of densities and are plotted in Fig. 3. It can be noted from the electric field dependence of these relative amplitudes, that, at a given temperature, the high mobility branch will extend to higher densities for higher field strengths. It also can be inferred from this data that, at constant field, the high mobility branch will extend to higher densities as the temperature increases.

The correspondence between our helium data and the hydrogen data as shown in Fig. 2 (insert) is striking. The low mobility branch in hydrogen was attributed to the formation of H_2^- or H^- ions by the high energy radioactive source used, although there was some doubt in this regard by the authors, who also felt that self-trapped "bubbles" were a possibility.[5]

In the present experiment, where one does not expect the formation of negative helium ions[11] since a low energy electron source was used, the low mobility branch is due either to a "bubble" state or some negative ion impurity. As discussed later, we rule out the negative ion impurity as a possibility. This data, then, gives support to the contention that the low mobility branch observed in hydrogen is also due to "bubbles."

Assuming then, that "bubble" states give rise to the low mobility branch, we have calculated their radii at these higher temperatures using the semi-classical formula[5]

$$\mu_0^b = \frac{e}{6\pi\eta R}\left[1 + \frac{9\pi n}{4\eta R(z\pi MkT)^{1/2}}\right] \qquad (1)$$

where η is the viscosity, R the bubble radius, n the number density, and M the reduced mass between the bubble and a helium atom which we take to be just the mass of the helium atom. We obtain a radius of 4.2 Å at 77.3 K and 4.5 Å at 160.1 K, values which are somewhat too low when one considers that the radii are on the order of 12 Å to 20 Å in the liquid.[12,13] It is somewhat doubtful, however, whether one should use the helium mass for M in this case since the "bubble" mass need not be large compared to that of the helium atom.[6]

For several reasons, we believe that impurities do not play a measureable role in our present experiments. In the first instance, we used helium gas of two different purity levels without any noticeable differences in drift velocities. In the case of our two temperature runs, one would expect higher impurity levels and effects at 160.1 K than at 77.3 K; for example, any oxygen impurity would freeze out at 77.3 K but not at 160.1 K. Such an impurity ion would then give a low mobility signal over a much longer density range than we have observed.[7] Also, in regard to the relative peak amplitudes in the region of overlap shown in Fig. 3, the signal strength due to a negative ion impurity would increase in direct proportion to the density, an effect which has not been observed.

In order to obtain a theoretical estimate of the zero field mobilities of the upper branch, we have used a modification of the semi-classical formula for gases and liquids[14,5]

$$\mu_0^f = \{4e/3\sigma(2\pi mkT)^{1/2}\}(1+B_1 n) \qquad (2)$$

where m is the electron mass, B_1 the second virial coefficient and σ the s-wave scattering cross-section. At densities less than 1.0×10^{21} cm^{-3} our data agrees to within 20% of these theoretical values, but for higher densities this agreement becomes gradually poorer until at 3.0×10^{21} cm^{-3} these theoretical values are about 45% too high. Trapping due to fluctuations (pseudobubbles) would lower this theoretical estimate to essentially the observed value, but the point here is that these calculations do suggest that we are dealing with free electrons in the high mobility branch.

The primary implications that we have drawn from these experiments are that we have observed self-trapped bubbles in dense helium gas at high temperatures and pressures and that we have observed the coexistence of free electron and "bubble" states over a significant density range (where quite probably, coexisting free electrons and pseudobubbles lead to the high mobility branch and self-trapped states lead to the low mobility branch). This interpretation further suggests that we are dealing with a nonequilibrium phenomenon (because of the branching) implying a long relaxation time to the low mobility states. This is of some interest in view of the short lifetimes observed in the liquid[8] and in view of the intermediate mobilities observed at lower temperatures where fast relaxation due to fluctuation trapping gives rise to thermal equilibrium between free and pseudobubble states. It may be that the number and trapping cross sections of the states observed here are quite strongly dependent on density and temperature, giving rise to a longer trapping time than that found at lower temperatures. If one were to obtain a longer drift time by the use of a longer drift space or a lower electric field, one would expect, in this view, that the free electron signal strength would decrease with a corresponding increase in the "bubble" signal. This change has indeed been observed as is shown in Fig. 3.

From the data of Harrison and Springett[4] for helium at 18 K, we had expected a gradual decrease in mobility at our higher temperatures rather than branching. It is possible that branching also occurs at these lower temperatures but was not detected by the single gate technique. We are presently extending our experiments to lower temperatures in order to draw some consistency between these two sets of data.

The authors wish to thank J. P. Hernandez for many helpful discussions and P. Smejtek and T. Carruthers for their experimental advice.

REFERENCES

1. T. P. Eggarter, Phys. Rev. A5, 2496 (1972); T. P. Eggarter and M. H. Cohen, Phys. Rev. Letters 25, 307 (1970); T. P. Eggarter and M. H. Cohen, Phys. Rev. Letters 27, 129 (1971).
2. J. P. Hernandez, Phys. Rev. A5, 635 (1972).
3. J. L. Levine and T. M. Sanders, Jr., Phys. Rev. 154, 138 (1967).
4. H. R. Harrison and B. E. Springett, Physics Letters 35A, 73 (1971).
5. H. R. Harrison and B. E. Springett, Chem. Phys. Letters 10, 418 (1971).
6. J. P. Hernandez (to be published).
7. J. A. Jahnke, [illegible]. Meyer, and S. A. Rice, Phys. Rev. A3, 734 (1971).
8. D. G. Onn and M. Silver, Phys. Rev. 183, 259 (1969).
9. D. G. Onn, P. Smejtek, and M. Silver, Boulder Low Temperature Physics Conference XIII 1972. Details of the use of this source in mobility experiments will be published in a subsequent paper.
10. R. D. McCarty and R. B. Stewart, Progress in International Research on Thermodynamics and Transport Properties. Academic Press, N. Y. (1962).
11. F. Reif and L. Meyer, Phys. Rev. 119, 1164 (1960).
12. B. E. Springett, M. H. Cohen, and J. Jortner, Phys. Rev. 159, 183 (1967).
13. R. M. Ostermeier and K. W. Schwarz, Phys. Rev. A5, 2510 (1972).
14. J. Lekner, Phys. Rev. 158, 130 (1967).

FIGURE CAPTIONS

Fig. 1 Electron Drift velocity versus electric field strength at 77.3 K in a pressure range of 10 Kg/cm^2 to 40 Kg/cm^2. The drift velocity is nonlinear at 100 V/cm at pressures less than 10 Kg/cm^2.

Fig. 2 Zero-field electron mobilities as a function of number density in dense helium gas. The dashed lines represent the earlier data of Harrison and Springett for helium. The inset compares our 77.3 K data for helium with the hydrogen data of Harrison and Springett at 31.7 K. Note the existence of high and low mobility branches in both cases.

Fig. 3 Relative signal strengths of the high and low mobility branches versus number density at 77.3 K and 160.1 K. The figure for 77.3 K also shows the effect of the electric field on the relative intensities. The data for 160.1 K was taken at a field of 100 V/cm.

FIGURE 1.

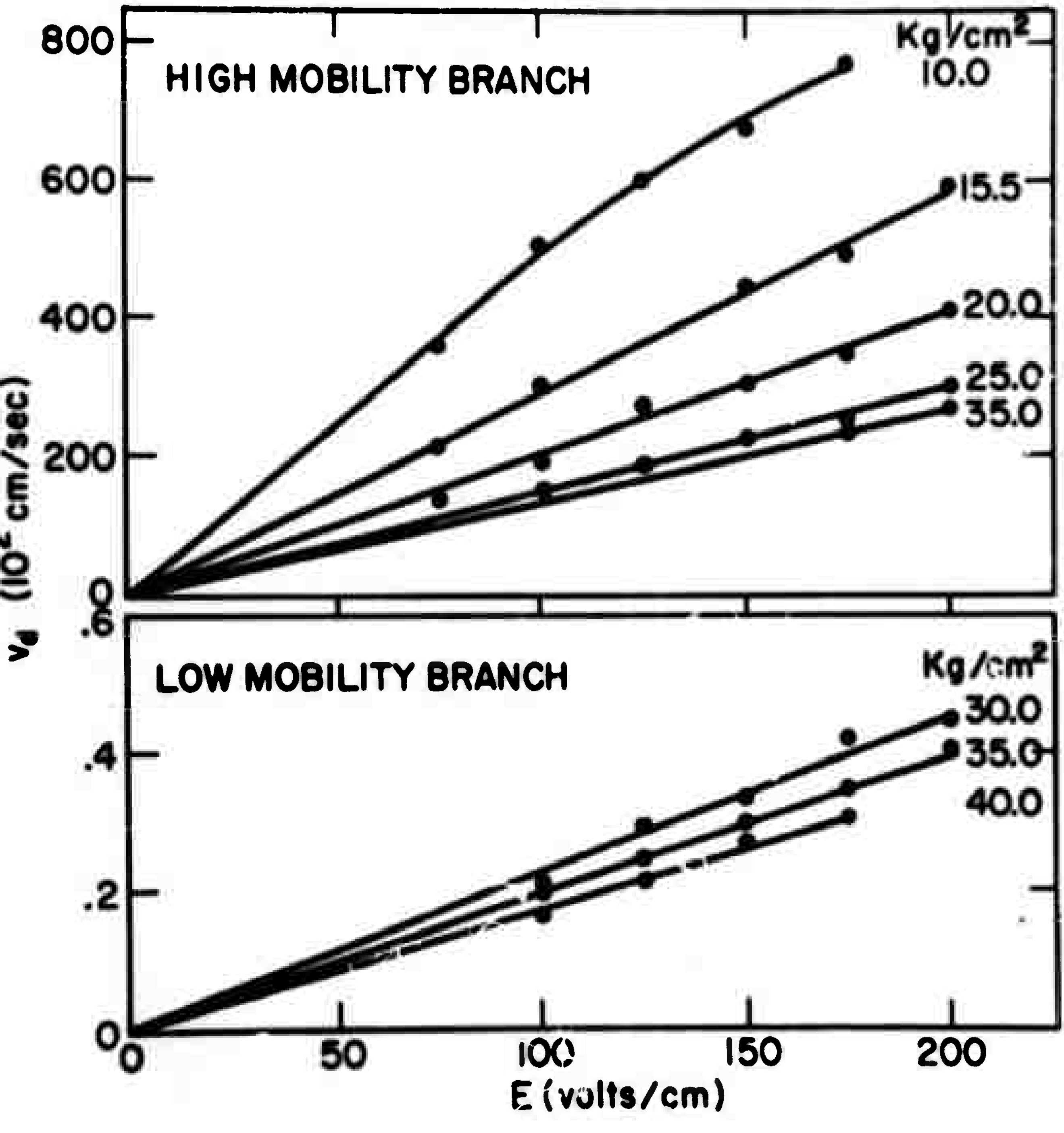

HIGH MOBILITY BRANCH
Kg/cm²
10.0
15.5
20.0
25.0
35.0
LOW MOBILITY BRANCH
Kg/cm²
30.0
35.0
40.0
v_d (10^2 cm/sec)
E (volts/cm)

FIGURE 2

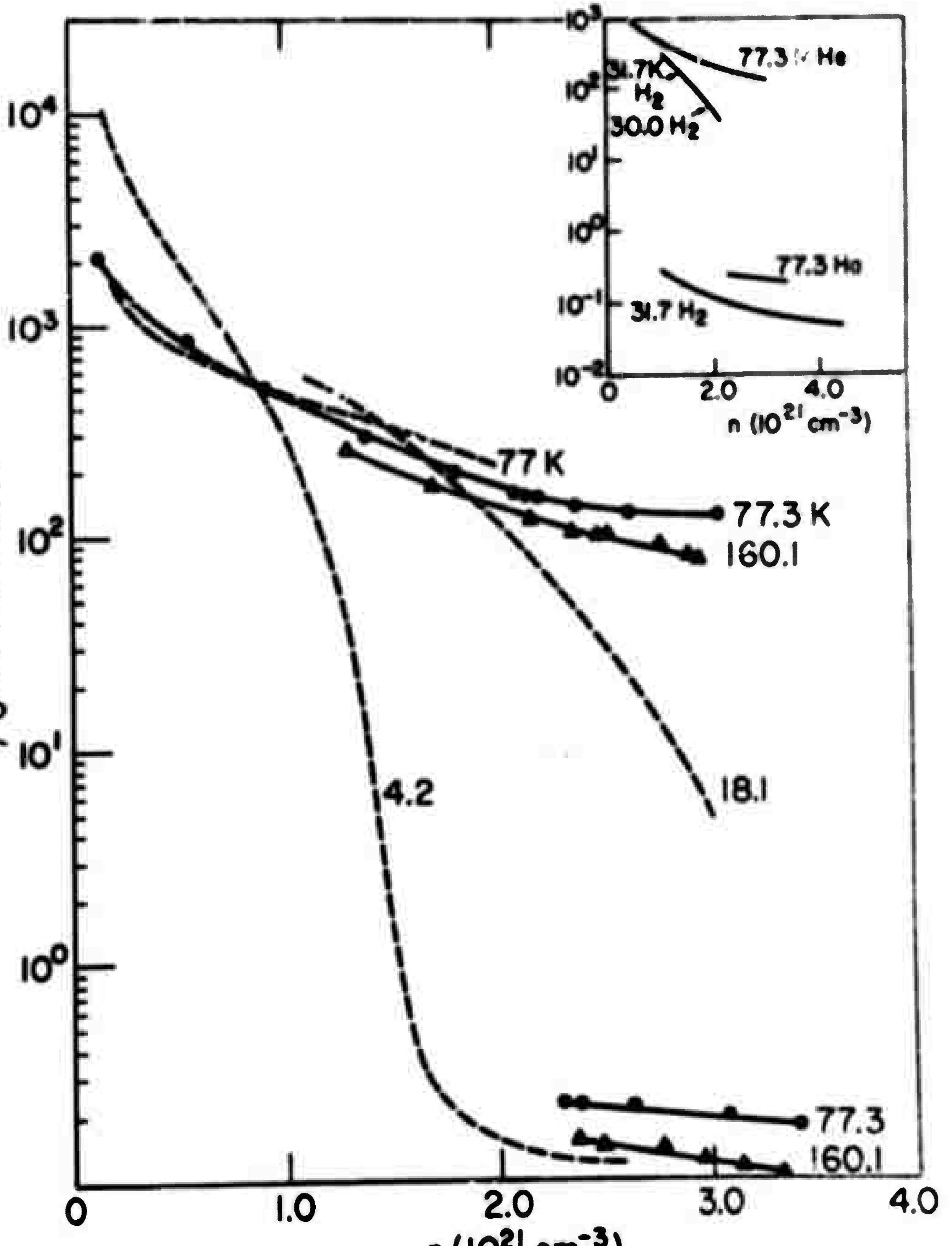

10^4
10^3
10^2
10^1
10^0
μ_D (cm^2/volt-sec)
77 K
77.3 K
160.1
4.2
18.1
77.3
160.1
0
1.0
2.0
3.0
4.0
n (10^{21} cm^{-3})
77.3 K He
31.7K
H_2
30.0 H_2
77.3 He
31.7 H_2

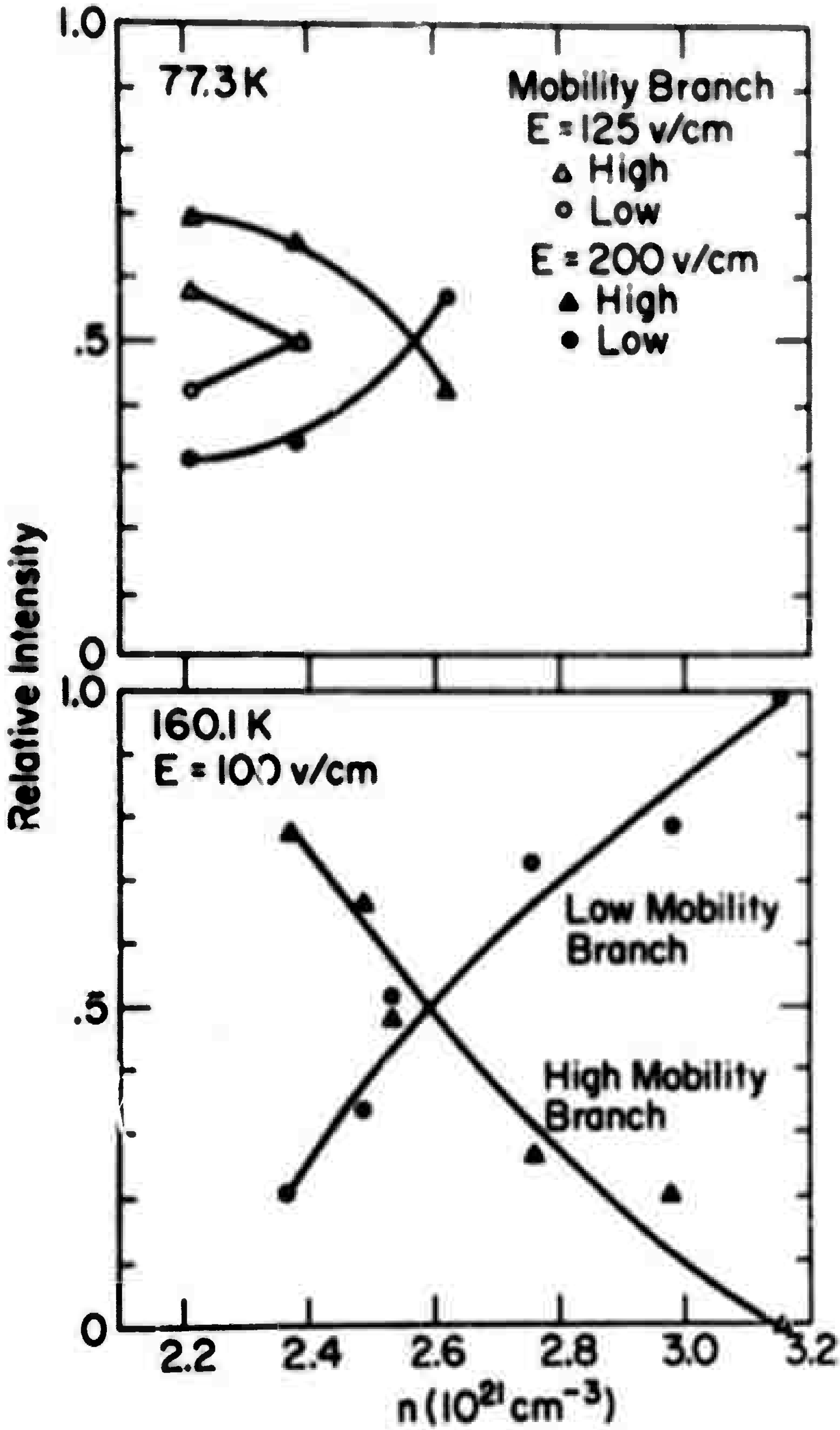
1.0
77.3 K
Mobility Branch
E = 125 v/cm
△ High
○ Low
E = 200 v/cm
▲ High
● Low
.5
0
Relative Intensity
1.0
160.1 K
E = 100 v/cm
Low Mobility Branch
High Mobility Branch
.5
0
2.2
2.4
2.6
2.8
3.0
3.2
n (10^{21} cm^{-3})